1998

Bimaterial interfacial failure investigation through the use of the constrained blister test

Gary Charles Neumeister
Lehigh University

Neumeister, Gary Charles

Bimaterial Interfacial Failure Investigation Through the Use of the Constrained Blister Test

May 13, 1998

BIMATERIAL INTERFACIAL FAILURE INVESTIGATION THROUGH THE USE OF THE CONSTRAINED BLISTER TEST

BY

GARY CHARLES NEUMEISTER

A THESIS

PRESENTED TO THE GRADUATE COMMITTEE

OF LEHIGH UNIVERSITY

IN CANDIDACY FOR THE DEGREE OF

MASTER OF SCIENCE

IN

POLYMER SCIENCE AND ENGINEERING

LEHIGH UNIVERSITY

1998

CERTIFICATE OF APPROVAL

This Thesis is accepted and approved in partial fulfillment of the requirements for the degree of Master of Science in Polymer Science and Engineering.

4 May 1998
DATE

_____
Thesis Advisor

_____
Department Chairperson

_____
Polymer Science and Engineering Chairperson

TABLE OF CONTENTS

LIST OF TABLES

LIST OF FIGURES

LIST OF APPENDICES

ABSTRACT

The investigation of the failure of a ductile-to-ductile bimaterial interface, through use a non-dimensional critical decohesion parameter model was undertaken. The constrained blister test was utilized to investigate the effects of environmental exposure on a DEGBA epoxy / 2024-T3 aluminum bimaterial interface for several coating thicknesses. Strain energy release rates G_{ic}, generated from the constrained blister test, were determined to range from a high of 225 J/m^2 for the thickest epoxy coating (0.6604 mm) to 105 J/m^2 for the thinnest - successfully tested (0.2540 mm) - unexposed specimens. G_{ic} values for the longest exposure (60 hours) ranged from a high of 115 J/m^2 to a low of 28 J/m^2. A dependence of G_{ic} to boiling-water exposure time, and coating thickness was found, with G_{ic} decreasing as exposure times increased, and increasing with increased coating thickness. Trends in critical decohesion number as a function of coating thickness and environmental exposure were also established. As with the experimentally determined G_{ic} data, the critical decohesion numbers followed two distinct trends; a dependence of Ω_c on boiling-water exposure time, and a dependence of Ω_c on coating thickness. Increased exposure times, as well as increased coating thickness, lead to decreased critical decohesion numbers throughout the thickness range investigated. Ω_c values varied from a high of 6.01 (unexposed, 76.2 μm specimen) to a low of 1.01 (24 hour exposure, 355.6 μm specimen), with the majority of points falling in the 1 to 3 range.

1. INTRODUCTION

Adhesively bonded joints have become increasingly popular in engineering applications, and in turn the structural integrity of such components have become an important design guideline. The use of continuum fracture mechanics is an established method for the assessment of the service lifetime of homogeneous materials and structures, and has been used in the design and service life prediction adhesive joints - assuming strictly adhesive failure. The application of fracture mechanics to the cohesive fracture of adhesively bonded joints is more complex than that of homogeneous materials, with the most severe problems encountered when interfacial failure is the dominate failure mechanism. Crack growth along the adhesive (coating) / substrate interface is of major importance, and environmental attack upon this interface is often a precursor to joint / coating failure.

The integrity of bimaterial interfaces is also of significant concern to the electronics industry. Multilayer circuit boards with their sandwich-type construction consist of alternating layers fiber glass reinforced epoxy and metallic (copper) foil. This construction leads to a multitude of bimaterial interfaces which are prone to cohesive failure, which in turn can ultimately lead to device failure.

Despite the importance of these bimaterial interfaces, only a relatively small amount of work has been dedicated to the characterization and understanding of their failure criteria. The development of an effective means of measuring this failure criteria, and its subsequent application to a proven coating decohesion model, would advance the state of understanding for these important interfaces.

1.1 BACKGROUND

In order to better understand the decohesion of bimaterial interfaces, it is useful to review some of the previous work focused on the study of interfacial failure mechanisms. We will start with a brief look at recent bimaterial interfacial fracture work performed by conventional testing methods such as the double cantilever beam and micro-indentation tests. We will then switch our focus to the various forms of the blister test, and how each was used to investigate the interfacial failure process of bimaterial interfaces.

1.1.1 Conventional Testing

Smith, Kramer, Xiao, and Hui[1] evaluated polymer-nonpolymer adhesion in terms of the fracture toughness of the interface using asymmetric double cantilever beam testing geometry. Tests were conducted on polystyrene(PS)-glass, PS-silicon (native oxide) modified by PS-poly(2 vinylpyridine)(PVP) and PS-poly methyl methacrylate (PMMA) diblock copolymers. It was found, that unlike tests such as the peel test whose results are strongly influenced by the stiffness and overall ductility of the polymer, the mechanics of the sandwich double cantilever beam test depends on the property of the glass and the local deformations at the crack tip and are independent of the bulk properties of the polymer. Therefore, with this testing configuration, it was postulated that it should be possible to compare the interfacial toughness of a much broader range of polymers using the same testing conditions. The PS-glass specimens showed that through careful control of the mixity of the

asymmetric sample, the crack trajectory could be biased toward the interface, and interfacial fracture assured.

Kinloch, Trusabanjong, and Williams[31] investigated the failure of adhesive joints which were modelled as a bimaterial interface consisting of an epoxy adhesive bonded to an aluminum substrate. Tapered double cantilever beam (TDCB) and symmetrical bimaterial (SBM) specimens were used for this effort. It was shown that only when residual stresses are present after cure of the adhesive layer is interfacial failure observed. The advancing crack always diverted into the adhesive layer prior to joint failure, and the higher the post-cure temperature of the adhesive (the higher the residual thermal stresses), the longer the interfacial crack traveled prior to diverting into the adhesive layer.

Thurston and Zehnder[2] conducted experiments wherein a range of mixed-mode loadings were applied to ceramic-metal sandwich specimens in order to determine the interfacial fracture toughness of a representative fused silica/copper system. This method was found to have several advantageous features including: (1) the existence of an analytical solution relating the bimaterial stress intensity factors to those for the corresponding homogeneous problem, (2) a specimen geometry which allows the shift in phase of the near-tip stresses with respect to the phase of the far-field stresses to be small at most angles; allowing for the determination of fracture toughness as a function of mixity over the complete range of phase angles, (3) the choice of sandwich

specimen geometry is designed to minimize the influence of residual stresses on the interfacial toughness.

Choi and Kim[3] focused their efforts in the analysis of the spontaneous decohesion of polyimide film on glass substrates. Spontaneous delamination was induced in specimens by a cut (after curing) in the thin film attached to the substrate. The delamination was driven by the residual stress caused by thermal strain mismatch between the film and substrate. This test allowed them to discriminate between the critical energy release rate for different fracture modes; in particular, it allowed for the determination of the effect of mode 3 mixity. From the measured shape of the delamination, interfacial fracture criteria were examined. Both numerical and experimental studies were used to confirm results which showed that the polyimide-glass interface is much tougher ($\approx$ 15.5 J/m^2) in the anti-plane shearing mode (mode 3), than in the tensile opening mode (mode I) ($\approx$ 4.3 J/m^2).

Zhang and Lewandowski[4] utilized microindentation to investigate the interfacial fracture toughness of Nb_5Si_3/Nb and Al/Al + 15% SiC reinforcement. Specimens were edge indented near the interface. The Al/Al composite interface stayed intact, while the Nb_5Si_3/Nb interface was found to debond under similar condition, indicating a much weaker interface. Interfacial delamination length was determined to be a function of the indenter load, and when the log-log plot of indenter load against interfacial crack length, the power-law relationship for interfacial fracture toughness, Ki was found to follow the model:

$$K_i = \gamma \frac{P}{e^{1.5}} \qquad (1a)$$

where γ is a fitting constant, P is the indenter pressure, and e is the interfacial crack length.

Evans and Hutchinson[5] investigated the mechanics of the delamination and spalling of compressed films using a combination of fracture mechanics and post-buckling theory. They demonstrated that the delamination of pre-compressed films could only occur if the film buckled, whereupon a stress intensification developed at the buckle perimeter. This stress intensity was found to depend on the magnitude of the prestress, σ_0, and the film thickness, t, such that a critical value of the quantity, $\sigma_0\sqrt{t}$ must be exceeded before the delamination can propagate. Additional work[6] analyzed interface to interface contact- effects on interface fracture resistance. Their work indicates that a simple zone model without friction predicts trends with the phase angle of loading which are qualitatively consistent with experimental results for a brittle-brittle interface (no plasticity associated with crack propagation).

1.1.2 Blister Test Efforts

Hinkley[7] examined the detachment of polystyrene and polymethyl methacrylate films from silicon substrates by using the conventional blister test. He found the test offered good reproducibility and exhibited the ability to distinguish quantitatively the interfacial adhesive strengths of glassy polymer films. His work focused on the alteration of the surface chemistry of silica, and the effects it had on the

measured energies of detachment; with values determined in the lab correlating well with theoretical values.

Gent and Lewnadowski[8] focused their efforts on an analysis of the critical internal pressure, P, at which a conventional blister will grow in size, in terms of the tensile modulus, E, and thickness, t, of an adhering layer, and the strength G_a of its adhesion to a rigid substrate. The detachment energy was determined to follow the function: $G_a = 0.65(P)(y)$, where y is the maximum deflection of the blister. Experimental results on pressure-sensitive tapes having significantly different effective modulus and thickness, were reported to correlate well with this model.

Jensen[9] utilized the convensional blister test to investigate interface fracture toughness for thin films bonded to an elastic substrate. Results from his efforts include energy release rates, and mixity of mode 1 and 2 for interface cracks where initial debonds extended several film thicknesses. Analytical results were determined for two extremes; very small film deflections (weak interfaces) and very large film deflections (tough interfaces). Additionally, numerical results were determined for intermediate conditions based on non-linear von Karman equations.

Jiang and Penn[10,11] modified the traditional blister test for use with brittle or fragile adhesives which exhibit early cohesive failure during pressurization, preventing the measure of the interfacial fracture energy. In their system, the substrate is the continuous top sheet (normally the substrate is the bottom plate with the pressurization

hole drilled in it), and the brittle adhesive (ice in their work) is in the form of a thin interlayer under the substrate, but mounted to a massive inert base through which the pressure is delivered. Interfacial fracture energy, F, was determined for ice adhering to a series of substrates. Fracture energies obtained were compared with work of adhesion values measured for water on the same substrates. Fracture energy, which contains both a reversible contribution due to intermolecular interactions across the interface (work of adhesion) and an irreversible contribution due to collective dissipative processes, was found to rise rapidly with modest increases in work of adhesion. This finding sugests that the irreversible contribution to fracture energy is influenced strongly by the intermolecular interactions at the interface.

Liechti and Liang[12] studied the crack initiation characteristics of bimaterial and sandwich strip blister specimens. Interface cracks were grown along glass/epoxy interfaces and the corresponding loads, normal crack opening displacements (NCOD), and crack front geometries were measured. Finite element analysis was used to compare NCODs, extract fracture parameters and examine near front stress fields. The phase angle dependence of toughness in the bimaterial specimens was found to be similar to that obtained in previous blister tests, but was much steeper than otherwise had been measured. The toughness of the glass/epoxy interface decreased with decreasing epoxy thickness, in spite of the fact that it was never completely spanned by plastic zones.

Chu and Durning's[13] work was aimed at investigating the fracture energy, G_a, of the interface between two incompatible polymers. Specifically, a solid, glassy polymer substrate (poly (methylmethacrylate))with a thin rubbery overcoating (polyisoprene) in which the blister was grown. An energy balance analysis was used to relate the time dependence of the debonding pressure, P, the blister radius, a, and the blister height, y, during tests carried out at constant fluid injection rates. They predict that after debonding initiates, P^{-3}, a^3, and y^3 are linear in time t, and that the slopes of these linear relationships are directly related to adhesion energy. One very interesting conclusion they reached was that the self-consistency of the fracture energies calculated in their work suggests that G_a can be calculated reliably from pressure data alone without using the blister geometry - the most difficult value to measure.

Jeong and White[14] studied the interfacial fracture energy between a thin polyimide film and a rigid Si substrate via the conventional blister test. They incorporated a dynamic debonding mechanism, and modeled the processes through use of a nonlinear local energy balance technique. The majority of previous work utilized a static debonding mechanism, therefore, based their analysis on linear elastic models. Jeong and White maintain the advantages of the dynamic debonding technique are: (1) the dissipated energies which accompany the debonding process can be measured, (2) the mechanical properties of the films do not enter into the calculation of the adhesion

strength. This study demonstrated that a minimum value for adhesion energy, which compared favorably with estimated values of adhesion, was obtainable.

Allen and Senturia[38] proposed the island blister test as an adhesion test which allows the peel of thin, well-adhered films without exceeding the tensile strength of the film. A model for this annular peel indicates that even for systems of good adhesion, peel can be initiated at low enough pressures to prevent film failure by making the center island sufficiently small relative to the size of the film. They found that the peel data obtained from these island sites correlated well to the behavior predicted by a simple fracture mechanics analysis.

Dillard and Bao[36] investigated the merits of the peninsula blister test as an extension of the island blister test developed by Allen and Senturia. Their preliminary results using pressure sensitive adhesive (PSA) tape compared favorably to an analytical model developed to predict the strain energy release rate for this test specimen in which the adherend may be considered; a plate, a pre-stressed membrane, or a simple membrane. The analytical results suggest that the specimen type may be applicable to a variety of practical adhesive systems.

Napolitano and Moet[15] investigated the failure behavior of pressure sensitive adhesive tape through use of the constrained blister test. A constant energy of interfacial adhesion of 1.8 J/m^2 was determined for a rubber-based pressure sensitive adhesive on a copper substrate. An "active zone" was visualized through the

transparent backing, and deformation within the active zone was found to consist of cavitation and deformation of ligaments. Fracture of these ligaments caused the detachment front to advance. The investigators proposed that the rate of energy dissipation, D, reflects the resistance of the bond to time dependent deformation, and therefore, dictates the lifetime for this specimen geometry. A direct relationship between lifetime and the inverse of the rate of energy dissipation in the active zone, was suggested.

Liang, Bell, and Mehta[16] determined the fracture energy required to separate electropolymerized n-octyl maleimide-co-styrene polymer films from various copper substrates using the constrained blister test. A strain energy release rate of 75 J/m^2 was found for separation of the polymer film from a smooth copper substrate. It was also determined that rough copper surfaces having a regular pattern substantially increased the adhesion strength of the polymer coatings.

Chang, Lai and Dillard[32] investigated the use of the constrained blister test to allow for a nearly constant strain energy release rate tests of adhesive bonds to be performed. Their preliminary effort focused on the evaluation of time-dependent adhesive fracture toughness of scotch tape, and highlighted the potential usefulness of the test method for investigation of viscoelastic and environmentally-assisted debonding processes. To solidify their position, analytical efforts[41] were undertaken to model the strain energy release rate of the constrained blister specimen, and to

correlate it with experimental values. The results of the finite element analysis confirmed the applicability of elementary plate theory to the constrained blister test.

1.2 DECOHESION PARAMETER MODEL THEORY

It has been shown that thin coatings of metals, ceramics, and polymers are, regularly, subject to sizable induced residual stress.[17,18] This stress can interact with small interfacial flaws inducing coating/substrate separation. This process, known as decohesion, is controlled by a non-dimensional critical decohesion number, Ω_c, which has been shown to follow the relationship:

$$\Omega_c = K_c / \sigma_0 \sqrt{h} \tag{1}$$

where K_c is the fracture resistance of the interface, σ_0 is the residual stress in the coating, and h is the coating thickness[19,20,21,22], for several coating/substrate combinations. The magnitude of the interfacial fracture resistance, and consequently the critical decohesion number, Ω_c, depends on the type of residual stress (tension versus compression), coating ductility, substrate ductility, and the relative moduli of the coating and substrate materials. The known modes of decohesion are summarized in Table 1.

Table 1 - Modes of Thin Film Decohesion

RESIDUAL STRESS	FILM TYPE	SUBSTRATE TYPE	INTERFACE BONDING	DECOHESION MECHANISM
Tensile	Brittle	Brittle	Poor	Edge decohesion @ interface (higher toughness film) Film cracking → interface decohesion
Tensile	Brittle	Ductile	Good	Film cracking: no decohesion

			Poor	Film cracking → interface decohesion
Tensile	Ductile	Brittle	Good Poor	Edge decohesion in substrate Edge decohesion at interface
Tensile	Ductile	Ductile	Good Poor	Edge decohesion at interface Film/substrate splitting → substrate decohesion
Compressive	Brittle	Ductile	Good Poor	Buckle propagation in film Substrate splitting
Compressive	Brittle/ Ductile	Brittle	Good Poor	Substrate splitting Buckle propagation at interface
Compressive	Ductile	Ductile	Good Poor	No decohesion Buckle propagation at interface

For conditions of residual tension in the films, the behavior of adherent brittle films on brittle substrates is exemplified by results obtained for chromium films on glass substrates.[22] In this instance, decohesion involved film cracking, followed by cracking of the substrate to the interface. Studies focusing on decohesion for brittle substrate systems with adherent thin films possessing relatively high toughness (i.e. polymers on glass[23] and alumina on glass[24]) have also been undertaken. Decohesion in these instances initiate at specimen's edge, but eventually extends through the substrate parallel to the interface. Film fracture has also been studied in systems with adherent brittle films on ductile substrates, an example of which is chromium films on aluminum. In such systems, a multiplicity of parallel cracks propagate across the film at a critical stress.

Conversely, studies of films subjected to residual compressive stress have also been undertaken.[19,25] These studies have analyzed the buckling and post-buckling behavior of films above interface flaws. Experiments comparing predicted and

measured trends in decohesion (initiated from circular flaws at the interface) have shown self-consistent agreement for the case wherein both the film and the substrate are brittle in nature (i.e. ZnO on glass)[26].

The underlying fundamentals of the fracture process concern trends in the stress intensity factor K and the phase angle of loading ψ, which represents the mixity of shear and tensile displacement on the crack surface. For elastically homogeneous materials:

$$\varphi = \tan^{-1} \frac{K_{II}}{K_I} \tag{2}$$

where: K_I and K_{II} are the mode I and mode II stress intensity factors, respectively. Film decohesion studies have established that film and substrate cracking always proceed along crack trajectories where $\varphi = 0$.[22,24] Consequently, K_c in Equation (1) is the Mode I (opening) value, K_{Ic}.

1.3 FRACTURE MECHANICS BASICS[27]

1.3.1 Energy Balance Approach

Two separate but complementary positions outlining the requirements for fracture have been proposed by Griffith[28] (and Orowan[29]) and Irwin. Griffith's[30] work supposes that fracture occurs when sufficient energy is released (from the stress field) by growth of the crack to supply the energy requirements of the new fracture

surface. The energy released comes from the stored elastic or potential energy of the loading system and can, in principle, be calculated for any type of test piece. This approach, therefore, provides a measure of the energy required to extend a crack over unit area and is termed the *fracture energy* or critical strain energy release rate and is denoted as G_c.

The quasi-static crack propagation can be viewed as the conversion of the work done (W_d) by an external force and the available elastic energy stored in the bulk of the specimen (U) into surface free energy (γ_m) following the relationship:

$$\frac{\partial(W_d - U)}{\partial a} \geq \gamma_m \frac{\partial A}{\partial a} \tag{3}$$

where ∂A is the increase in surface area associated with an increment of crack growth ∂a. For a crack propagating in a specimen of thickness, b, the above becomes:

$$\frac{1}{b} \cdot \frac{\partial(W_d - U)}{\partial a} \geq 2\gamma_m \tag{4}$$

The value of $2\gamma_m$ is equivalent to W_A (work of adhesion) in the case of crack growth along an interface, since it only reflects the energy required to rupture secondary bonds such as van der Waals forces. Crack growth in materials, as well as along interfaces, often requires the breaking of stronger forces such as primary bonds. Additionally, fracture in even extremely brittle adhesives involves localized viscoelastic and/or plastic energy disipative processes occuring where high strains are experienced (i.e.

crack tips). Such micromechanisms represent the main source of energy absorption in the material.

If it is assumed that energy dissipation around the crack tip occurs in a manner independent of test geometry or force application, then $2\gamma_m$ in Equation 4 can be replaced by G_C, which incorporates all the energy losses incurred around the crack tip and is, therefore, the energy required to increase the crack by unit length in a specimen of unit width. The fracture criterion now becomes:

$$\frac{1}{b}\cdot\frac{\partial(W_d - U)}{\partial a} \geq G_c \tag{5}$$

For bonded structures exhibiting bulk linear-elastic behavior (obey Hooke's Law), Equation 5 can be expressed as:

$$G_c = \frac{F_c^2}{2b}\frac{\partial C}{\partial a} \tag{6}$$

where F_C is the load at the onset of crack propagation and C is the compliance of the structure. For an infinitesimally small amount of crack growth, this equation is valid for a cracked body under fixed-extension or constant-load conditions. This equation is the foundation of many calculations of G_C since if C is determined as a function of a, then $\partial C / \partial a$ can be determined. Therefore, if the load, F_C, at the onset of crack growth is measured for a known crack length, a, then the value of G_C may be deduced.

Advantages of this energy balance approach are firstly, the unambiguous determination of G_C from Equations 5 and 6. This is true whether a thin or thick adhesive layer is employed and whether the crack propagates deep in the adhesive layer or at or near the interface. Secondly, the value of G_C may be related to the intrinsic bonding forces (G_O) in the material, or that acting across the interface. From the first law of thermodynamics the following relationship can be written:

$$G_c = G_o + \psi \tag{7}$$

where ψ is the energy dissipated in viscoelastic and plastic deformation at the crack tip. The value of ψ is usually the major contribution to the value of G_C, and it is this parameter which frequently results in the measured value of G_C being highly dependent upon the rate and temperature of testing.

Gent, Kinloch, Andrew and Shultz proposed the following relationship based on the afore mentioned relationship:

$$\psi = G_o f(a,T,\varepsilon) \tag{8}$$

where f is a function whose value depends upon the crack growth, a, test temperature, T, and strain level, ε. Combining of Equation 7 and 8 yields:

$$G_c = G_o(1 + f(a,T,E)) \tag{9}$$

A *loss function* (Φ_v) can now be defined as the following:

$$\Phi_v(a,T,\varepsilon) = 1 + f(a,T,\varepsilon) \tag{10}$$

so that combining Equation 9 and 10 yields the following relationship:

$$G_c = G_o \Phi_v(a,T,\varepsilon) \tag{11}$$

The important outcome of Equation 11 is that when viscoelastic and plastic energy losses are negligible ($\Phi_v(a,T,\varepsilon) \to 1$, and $f(a,T,\varepsilon) \to 0$), the measured value of the fracture energy is equal to G_0 -intrinsic fracture energy.

In an adhesive joint the failure plane can be located either in the materials forming the couple or along the interface, or it may wander in and out of the two paths. Therefore, the value of the intrinsic fracture energy may be expressed as a weighted mean of the various possible failure paths:

$$G_0 = iG_0(\text{interfacial}) + b'G_0(\text{adhesive}) = sG_0(\text{substrate}) \tag{12}$$

where G_0(interfacial), G_0(adhesive) and G_0(substrate) are the intrinsic fracture energies for interfacial, cohesive-in-adhesive, and cohesive-in-substrate failure respectively, and i, b' and s are the respective area fractions of interfacial failure, failure in adhesive and failure in substrate.[27]

For specimens which exhibit solely interfacial failure the i=1, and the resulting value for G_0 from Equation 12 takes the same value as G_0(interfacial). If only secondary bonds are operating across the interface then the value of G_0 should be

equal to the value of the thermodynamic work of adhesion, W_A. Alternatively, if stronger interfacial forces are present (i.e. primary bonds) then the value of G_0 will be much greater than W_A.

In the simple case of interfacial failure involving the breaking of secondary bonds and a model viscoelastic adhesive, the relationships as shown in the previous equations have been shown to be valid. They also appear to be applicable to failure of model viscoelastic adhesives with failures occurring near the interface, or in bulk adhesive, with the fracture event requiring the rupture of primary bonds.

1.3.2 Stress Intensity Factor Approach

Irwin, on the other hand, found that the stress field around a sharp crack in a linear-elastic material could be uniquely defined by a parameter called the stress intensity factor, K, and that fracture occurs when the value of K exceeds some critical value, K_c. Therefore, K is a stress-field parameter independent of the material, whereas K_c - referred to as *the fracture toughness* - is a measure of a material property.

Assuming a sharp crack exists in a uniformly stressed, infinite sized, homogeneous material which exhibits Hookean behavior when exposed to infinitesimal strains, Westergaard developed models which relate the local stress-

concentration of stresses at the crack tip to the applied stress, σ_0. For the specific case of a region close to the crack tip the solution takes the form:

$$\sigma_{ij} = \sigma_o \left(\frac{a}{2r} \right)^{1/2} f_{ij}(\theta) \tag{13}$$

where σ_{ij} are the components of the stress tensor at a point, r and θ are the polar coordinates of the point, and 2a is the length of the crack. Irwin then modified Equation 13 to include the stress intensity factor, K, which relates the magnitude of the stress intensity local to the crack in terms of applied loading and specimen geometry as seen in Equation 14.

$$\sigma_{ij} = \left(\frac{K}{(2\pi\ r)^{1/2}} \right) f_{ij}(\theta) \tag{14}$$

A crack may be stressed in three different modes, denoted mode I (tensile opening, II (in-plane shear), and III (antiplane shear), as illustrated in Figure 1. Superposition of the three modes constitutes the general case of crack loading. The cleavage or tensile-opening mode - mode I - is technically the most important since it is the most commonly encountered and the mode most often resulting in failure.

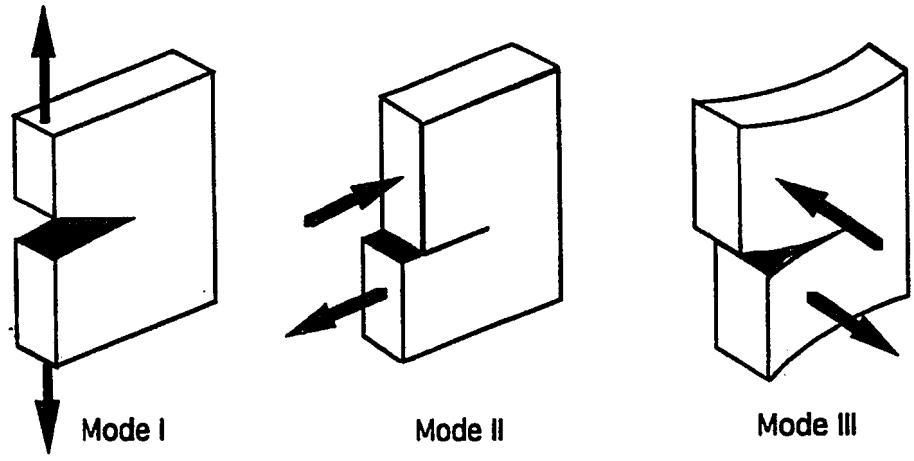

Figure 1 - Illustration of Crack Propagation Modes

For the case of mode I loading, the crack tip stresses may be developed from Equation 14 to give the following expressions:

$$\sigma_{11} = \frac{K_I}{(2\pi r)^{1/2}} \cos(\theta/2)(1+\sin(\theta/2)\sin(3\theta/2)) \tag{15}$$

$$\tau_{12} = \frac{K_I}{(2\pi r)^{1/2}} \cos(\theta/2)(\sin(\theta/2)\cos(3\theta/2)) \tag{16}$$

$$\sigma_{22} = \frac{K_I}{(2\pi r)^{1/2}} \cos(\theta/2)(1-\sin(\theta/2)\sin(3\theta/2)) \tag{17}$$

$$\sigma_{33} = 0 \qquad \text{-- Plane Stress} \tag{18}$$

$$\sigma_{22} = \nu(\sigma_{11}+\sigma_{22}) \qquad \text{-- Plane Strain} \tag{19}$$

$$\tau_{23} = \tau_{13} = 0 \tag{20}$$

As shown in Equations 15 through 17, as r$\rightarrow$ 0 the stress $\sigma_{ij} \rightarrow \infty$, and, therefore, stress alone is not adequate to predict local fracture criterion. Since the level of K_I

defines the stress field around the crack, Irwin proposed the idea that a $K_I \geq K_{IC}$ (critical value for crack growth), would suitably define a fracture criterion. This *fracture toughness* value is a material property which characterizes the intensity of the stress field ahead of a crack. The power of this approach is that for any mode I problem, K_I can always be expressed in the form:

$$K_I = Q\sigma_o a^{1/2} \tag{21}$$

and, therefore, K_{IC} in the form:

$$K_{Ic} = Q\sigma_c a^{1/2} \tag{22}$$

where σ_c is the applied stress at the onset of crack growth, and Q is a geometry factor whose makeup - in addition to geometric factors - may include; moduli and Poisson's ratios of the materials forming the interface. There is only very limited amounts of evidence that suggests the above treatment of fracture behavior of adhesive joints with cracks at or near an interface is valid.

The problem arises when a crack is at a bimaterial interface is subjected to tensile-only loads applied normal to the crack. This load will induce both tensile and shear loads around the crack tip, leading to a situation where both K_{Ii} and K_{IIi} (subscript "i" for interface) terms are required for the solution to the model. Unfortunately, these terms no longer have clearly defined physical significance, as

they did in the bulk material case outlined above.[31] Attempts to model the situation have yielded the relationship below:

$$\frac{f(K_{Ii}, K_{IIi})}{(2\pi r)^{1/2}}\begin{pmatrix}\sin\\ \cos\end{pmatrix}(\xi \ln r) \tag{22a}$$

where ξ is a "bimaterial constant" and is a function of the moduli and Poisson's ratios of the two materials forming the interface. Unlike the bulk material case, however, for the interface-crack case, stresses close to the crack tip are oscillatory, as are crack-face displacements, which leads to physically impossible solutions to the problem.

Because of these uncertainties, the majority of work has been focused on utilizing the energy balance approach when studying interfacial crack growth in bimaterial joints.

1.4 RELATIONSHIP BETWEEN G_{ic} AND K_{ic}

In the case of a bulk material, the relationship between the fracture energy, G_c, and the stress intensity factor K_c can be expressed (for plane strain condition) as:

$$G_c = \frac{(1-\nu^2)}{E}K_{Ic}^2 + \frac{(1-\nu^{2)}}{E}K_{IIc}^2 + \frac{(1+\nu)}{E}K_{IIIc}^2 \tag{23}$$

or in equivalent terms:

$$G_c = G_{Ic} + G_{IIc} + G_{IIIc} \tag{24}$$

where for mode I conditions:

$$G_{Ic} = \frac{K_{Ic}^2}{E}(1-\nu^2) \qquad \text{-- plane strain condition} \tag{25}$$

$$G_{Ic} = \frac{K_{Ic}^2}{E} \qquad \text{-- plane stress condition} \tag{26}$$

In the case of a crack at an interface no definitive relationship has been established. Several individuals have championed a method which utilizes a weighted average of the moduli of the materials forming the interface under question. The values of G_{ic} and K_{ic} (again i is for interfacial) can be related by:

$$G_{ic} = K_{ic}^2 \cdot \frac{1}{2}\left(\frac{1}{E_a}+\frac{1}{E_s}\right)\left(\frac{2\alpha_m - 1}{\alpha_m^2}\right) \tag{27}$$

where

$$\alpha_m = \frac{\xi + 1}{\chi + 1} \tag{28}$$

and

$$\xi = \frac{E_s}{E_a} \tag{29}$$

$$\chi = 1 + \frac{E_s}{2}\left(\frac{1+\nu_a}{E_a} - \frac{1+\nu_s}{E_s}\right) \tag{30}$$

1.5 MODE I FRACTURE MECHANICS SPECIMEN TEST GEOMETRIES[27]

Over the years, a large number of test geometries have been devised for evaluating the properties of bulk and in situ adhesives. Because typical adhesive

joints contain only a very small amount of adhesive, there is some question as to whether properties measured on bulk adhesive samples are meaningful in estimating the behavior of in situ adhesive material in a real application. ASTM has standardized a number of strength tests for bonded joints and yet the majority of these tests have very complex stress states. Although these tests offer standard ways to compare different adhesive systems or surface treatments, they do not yield properties which are appropriate from a design standpoint.[32]

A basic aim of fracture mechanics is to provide a parameter for characterizing crack growth which is independent of test geometry. In an attempt to accomplish this, a wide range of specimen geometries have been developed. Different geometries have also been developed in an attempt to obtain data under all three crack loading modes. Table 2 lists several tests designed to investigate Mode I fracture toughness within a bimaterial joint. The value of $\partial C / \partial a$ may always be determined experimentally, however, for several of the test geometries expressions for $\partial C / \partial a$ have been determined, and are included in the table.

Table 2 - Specimen Design for Mode I Fracture Toughness Investigation

GEOMETRY	EQUATION	INFORMATION
Double Cantilever Beam (DCB)	$G_{Ic} = \frac{F_c^2}{2b}\frac{\partial C}{\partial a}$ For thin adhesive layers: $\frac{\partial C}{\partial a} = \frac{8}{E_s b}\left(\frac{3a^2}{d^3} + \frac{1}{d}\right)$	Mode I. $\partial C / \partial a$ is not constant, and under a constant load G_I increases as "a" increases. d = height of substrate beam

Tapered Double Cantilever Beam (TDCB)	$G_{Ic} = \frac{4F_c^2 m_b}{E_s b^2}$ $m_b = \left(\frac{3a^2}{d^3} + \frac{1}{d}\right)$	Mode I. $\partial C / \partial a$ is constant, G_I independent of crack length.
Width-Tapered Beam	Same as above.	Mode I. $\partial C / \partial a$ is constant, G_I independent of crack length.
Double Torsion	$G_{Ic} = \frac{F_c^2}{2b}\frac{\partial C}{\partial a}$ For thin adhesive layers: $\frac{\partial C}{\partial a} = \frac{(1+\nu_s)}{E_s}\frac{2d_m^2}{k_7 db^3}$	Mode I. $\partial C / \partial a$ is constant, G_I independent of crack length.
Compact Tension	$K_{Ic} = \frac{F_c Q}{bD^{1/2}}$	Mode I
Independently Loaded Mixed-Mode	$G_{Ic} = \frac{4F_{Ic}^2}{b^2 d^3 E_s}\cdot\left[3(a+0.6d)^2 + d^2\right]$ $G_{IIc} = \frac{F_{IIc}^2}{b^2 d E_a}$	Cleavage and shear modes can be applied independently to produce either Mode I, Mode II or combinations of both.
Blister Test	$G_c = \left(\frac{1}{f(h_a/a)}\right)\left(\frac{p_{rc}^2 a}{E_a}\right)$	Largely Mode I, but Mode II increases as "a" increases. Value of G_{ic} is truly plain strain.

1.5.1 Double Cantilever Beam Specimen

The DCB and its variants have been more extensively used than other fracture tests. While appropriate for tests in inert environments, diffusion of species from a hostile environment along the sides of the specimens should preclude the use of this test for long term exposure conditions. It has been shown that consistent environmentally-degraded fracture energies from DCB specimens could not be obtained while the environment was ingressing the bond. Instead, the specimen had to

be conditioned long enough to achieve a uniform amount of bond degradation before testing could commence.[32]

1.5.2 Conventional Blister Test

The blister test was originally proposed by Dannenberg[33] for measuring the adhesion of coatings. In this test, a film is adhered to a substrate, one section of which has been removed, forming a hole which exposes the bottom surface of the film. Upon pressurizing the bottom surface, the film bulges up over the hole. If sufficient pressure is applied, the film will debond from the substrate and a "blister" will form, growing radially outward from the perimeter of the substrate hole as illustrated in Figure 2.[34]

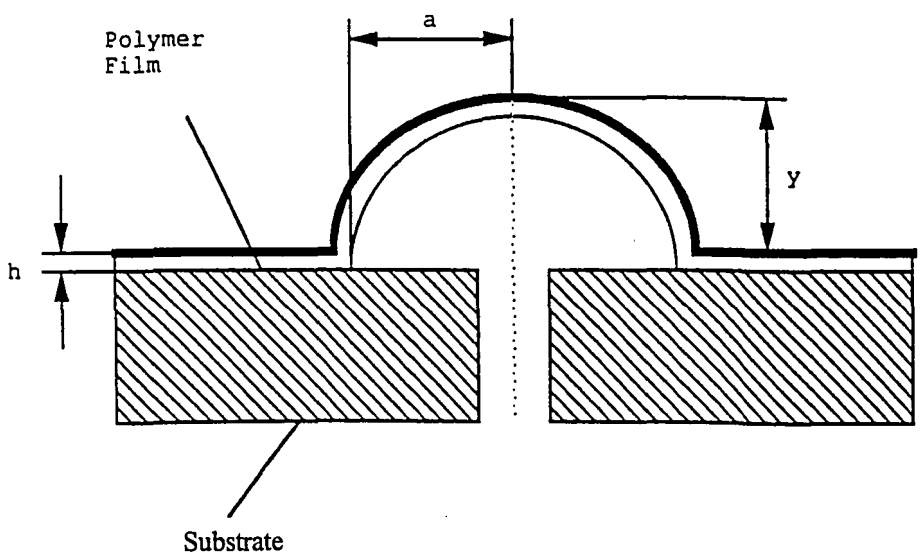

Figure 2 - Schematic Diagram of Blister Test Specimen

To permit better control over the debond growth, Dannenberg confined his blister by forcing it to form in a narrow groove, resulting in a constant strain energy release rate

specimen. Williams[35] later adapted the technique to measure the fracture energy of elastomeric materials adhesively bonded to a rigid substrate through incorporation of a circular debond.

The standard blister is extremely compatible with environmental exposures since the pressurizing medium is contained within the blister region. For circular versions of the blister specimen, the axisymmetric shape minimizes problems associated with edge effects of finite width specimens, and diffusion perpendicular to the debond front eliminates random effects for environmental exposure. One of the disadvantages with the standard blister is that the strain energy release rate increases with the fourth power of the debond radius, making accurate measurements of the debond essential, as well as conspiring to make a very unstable fracture specimen.[36] The blister test also suffers from the tensile strength limitations of the adherent. If films are thin and/or well-adhering, blisters may burst before crack propagation can be initiated. Despite this, the blister test offers several ways around the tensile strength limit - specifically in the form of the island blister test, the peninsula blister test, and the constrained blister test.

1.5.3 Island Blister Test

The island blister was proposed by Allen and Senturia[34] as a means to overcome the tensile strength limitation associated with the original unconstrained blister test. This technique is a modification of the standard blister site in that the

suspended membrane of film has an "island" of substrate still attached at its center (Figure 3).

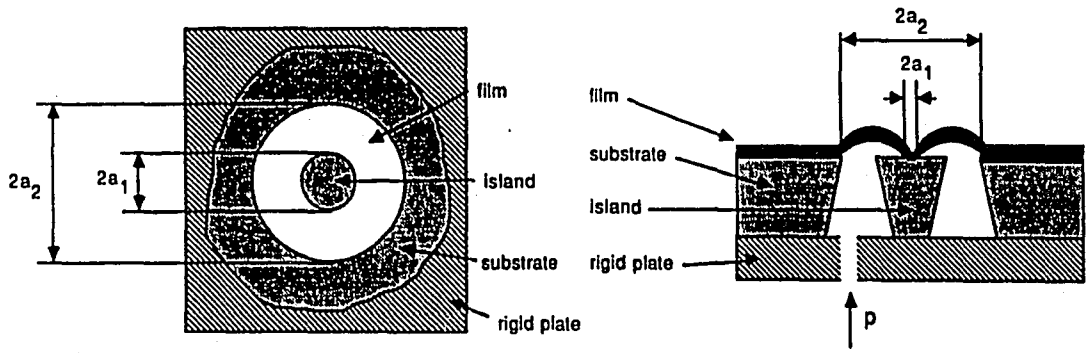

Figure 3 - Schematic Diagram of Island Blister Test Configuration

The island and the substrate are both fastened to a rigid plate and pressure is applied as in the standard blister test. Film peeling (crack growth) will now occur only off the center island. It has been shown[37] that the pressure necessary to initiate peel can be reduced to levels significantly below the tensile strength of the film by making the center island sufficiently small; thereby overcoming the tensile-strength limit of the films.

Several problems with this technique also exist. In order for the island blister test to be utilized it is necessary to keep the ratio of outer-to-inner radii arbitrarily large. This can most easily be achieved by fixing the island radius to a convenient size and increasing the outer film radius to the point that the film can be successfully peeled from the island - not always possible. Conversely, if substrate size limitations dictate a smaller specimen, then the ability to make a small (microscopic) island is

crucial to the success of this technique - again, not always possible.[38] Additionally, this method derives its high strain energy release rate from the fact that the debond front is reduced to a very small length. A moderate increase in compliance is produced by a relatively small increase in debond area, thereby giving rise to large strain energy release rates. As the membrane attachement site decreases in radius, the calculated strain energy release rate increases without bound.[36]

1.5.4 Peninsula Blister Test

In an effort to extend the concept of the island blister test, Dillard[36] *et al.* devised what is commonly referred to as the peninsula blister test. The name comes from the fact that the debonding occurs along a narrow "peninsula" which extends into the blister region as shown in Figure 4.

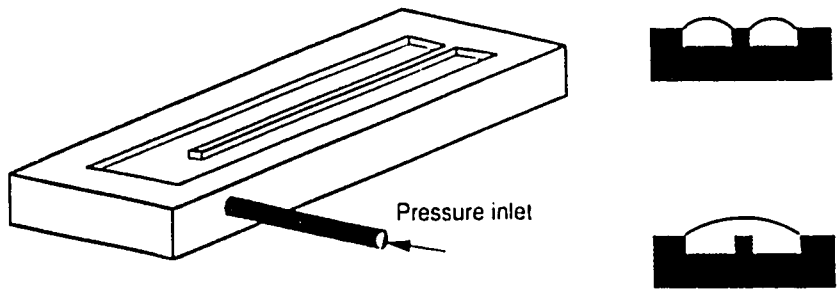

Figure 4 - Schematic Diagram of Peninsula Blister Test Configuration

Being similar to the island blister test specimen, the peninsula blister retains the advantageous high strain energy release rate for a given pressure - a prerequisite for testing adhesion of thin, delicate films. Unlike the island blister, however, the peninsula blister's strain energy release rate does not increase without bound as the debond area progresses; resulting in the highly desirable constant strain energy release rate state. Added features include the larger debond area, and additional data points that can be obtained from a single specimen. Disadvantages are that the fabrication of the specimne is difficult for certain material systems, and that the specimen is no longer axisymetric, thereby possibly reducing the utility for environmental exposure testing. There is also a mixture of mode I and mode II for the energy release rates, but the nature of this mixity has not been investigated.[36]

1.5.4 Constrained Blister Test

In the constrained blister test, the growing blister is constrained in the vertical direction by placing a plate over it (Figure 5).

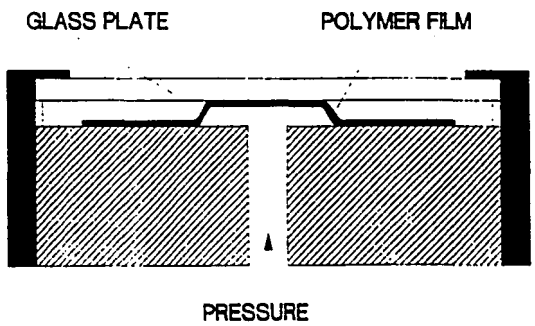

Figure 5 - Schematic Diagram of Constrained Blister Test Configuration

The plate prevents large deflections in the vertical direction, allowing large pressures to be applied to the blister without tearing the film.[38] Additionally, the constrained blister test significantly reduces the dependence of the strain energy release rate on debond radius, and can be operated under constant strain energy releases rates in limiting cases. Questions have arisen regarding the effect of friction between the adherend and the constraint, and although the numerical results[39] suggest that the effect is totally negligible, the difficulty of analyzing a contact problem with large deflections causes some concern.

1.6 THEORY BEHIND CONSTRAINED BLISTER TEST

One of the most difficult problems associated with the blister specimen is the determination of the debond radius. Measurement of the debond size is important for two reasons; the determination of the increments in crack growth, and the evaluation of the debond radius for calculation of the strain energy release rate. Anderson et al.[40] discussed closed form and numerical solutions for the strain energy release rate and have identified regions of applicability for formulae for a penny-shaped crack between two simi-infinite media and for plate theory. Assuming a thin plate with small deformations, the closed form solution is:

$$G = \frac{3(1-\nu^2)}{32Et^3} p^2 a^4 \tag{31}$$

where G is the strain energy release rate, v, E, and t are the Poisson's ratio, Young's modulus, and thickness of the blister adherend, p is the applied pressure, and a is the debond radius. Since the radius term appears to the fourth power, small errors in measuring the debond will result in significant errors in estimating G. Because of the difficulties in measuring the debond for opague adherends, a modified test with nearly constant G would facilitate experimental evaluation of adhesive toughness.[39]

A constant G test occurs when the compliance of a specimen increases linearly with crack area. To this end, a flat constraint can be placed above the blister to limit its displacement (Figure 5). Geometry shows (if the intermediate region where the blister is suspended between the substrates and the constraining plate is neglected) the volume under the blister will increase linearly with debond area. This implies that for a constant-pressure loading mode, the work done on the system is the incremental debond area multiplied by the distance the blister travels before reaching the constraint.

The classical energy conservation approach for the determination of strain energy release rates for adhesive bonds can be utilized to support the above supposition. In this approach, localized viscoelastic and plastic deformations in the vicinity of the crack tip are included in the critical strain energy release rate, G_c = $G_c(da/dt)$, making it a function of debond rate. This approach - in contrast with an

approach which assumes that G_c is an intrinsic fracture resistance of the material (dividing near and far-field effects into separate terms) - is considered acceptable due to the fact that near-field dissipation is not easily separated from the "inherent" surface energy.

When debonding occurs:

$$G_c \delta A = \delta W - \delta U - \delta Z \tag{32}$$

where G_c is the critical value of strain energy release rate which may be a function of debond rate and environment, δA is the variation in debond area, δW is the variation in external work done on the system, δU is the variation in stored elastic energy, and δZ is the variation in energy dissipated due to bulk viscoelastic and frictional effects. It has been show experimentally[32] as well as numerically[39] and analytically[41] that the variation in stored energy (δU) is negligible and can therefore be disregarded. Likewise, the δZ term can be neglected assuming that there is little far field viscoelastic dissipation in the blister adherend. These assumption allow for the following modifications to Equation 32:

$$G_c \delta A = \delta W = p \delta V \tag{33}$$

where p is the applied pressure and δV is the variation in volume under the blister. To approximate this variation in volume, the assumption is made that the suspended region of the blister is linear. Through use of the Theorem of Pappus[32], the volume is determined to follow the relationship:

$$V = \pi h\left(a^2 - ad + \frac{d^2}{3}\right) \tag{34}$$

Substituting Equation 34 into Equation 33, it is seen that the strain energy release rate is a product of the pressure, the contraint height, and a correction factor, q.

$$G_c = phq \tag{35}$$

Again assuming the suspended region of the blister is linear the correction factor, q is given by:

$$q = \left(1 - \frac{d}{2a}\right) + \left(\frac{d}{3a} - \frac{1}{2}\right)\frac{\partial d}{\partial a} \tag{36}$$

Since the detachement distance, d, changes only slightly as the debond grows, the partial derivative has been shown to negligible.[39] There is, however, a dependency on the relative sizes of the debond radius to the detached zone.[32] When the relative size of the detached zone is not small, there is some variation in G with debond distance. This variation can be accurately estimated through the use of Equation 36.[39] The variation of q with the ratio a/d as determined by Chang, Lai, and Dillard[32] is presented in Figure 6. The correction factors were found to be even closer to unity if the detached region has some curvature induced by the pressure, as is typically observed with flexible adherends.

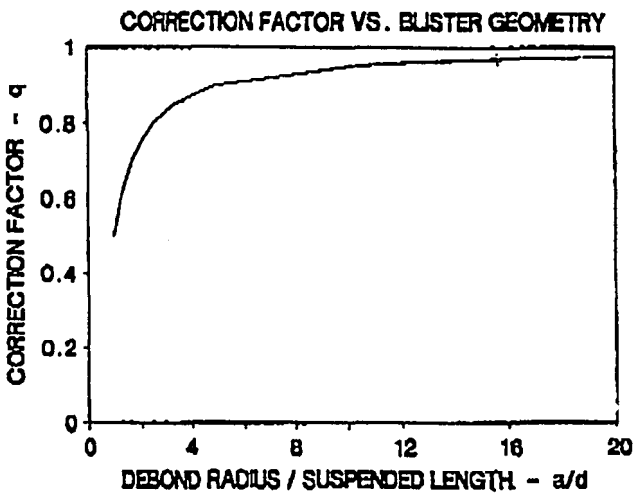

Figure 6 - Correction Factor, q, Plotted as a Function of a/d Ratio

1.7 OBJECTIVE

The objective of this research is to investigate the bimaterial interfacial failure of a ductile adherent on a ductile substrate, through use a non-dimensional critical decohesion parameter model originally developed for use in brittle to brittle bimaterial interfacial fracture work. The constrained blister test was utilized to investigate the effects of environmental exposure on a DEGBA epoxy / 2024-T3 aluminum bimaterial interface for several coating thicknesses. Strain energy release rates G_{ic} were determined from data generated from the constrained blister test, and then converted to fracture toughness K_{ic} values through use of a weighted bimaterial modulus, ξ. Residual stresses present within the specimen after cure were numerically determined through the use of a modified plate theory analysis. Finally, these values were inserted into the critical decohesion number model, and trends of

decohesion number as a function of coating thickness and environmental exposure for a ductile / ductile bimaterial interface were established.

2. EXPERIMENTAL

2.1 MATERIALS

The substrate material utilized throughout this work was 2024 aluminum in the T3 condition. This ductile solution heat treated, naturally aged alloy is customarily used in the manufacture of aircraft components, and as such, is often a key material in adhesive bonding investigations. All testing was conducted using 0.68 mm sheet stock.

The adherent used throughout this work was a two part system consisting of Dow Corning's DER 332™ thermosetting epoxy resin and Air Products Amicure™ PACM curing agent. DER 332™ is in the diglycidylether of bisphenol A (DEGBA) family of amine resins, which maintains a tighter molecular-weight-distribution when compared to the chemically-similar Epon 828™ resin from Shell. The PACM curing agent is an unmodified cycloaliphatic amine; chemically Bis(p-amino-cyclohexyl)methane (Figure 7) which is used the ratio of 28g per 100 g. of epoxy resin.

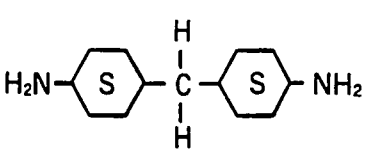

M.W. - 210
Eq. Wt. 52.2
phr for Epon resin 828-28
Viscosity, 25°C, Pa·s (poise)
0.006 (0.06)

Figure 7 - Amicure PACM Information

This model epoxy resin system was chosen for this study because of its well characterized nature, relatively forgiving processing window, and broad-based applicability.

2.2 MATERIAL PREPARATION

Adherent: Prior to mixing, both components were degassed under full vacuum. The DER 332 was degassed at 80°C until bubbling ceased; the lower viscosity PACM was similarly degassed at room temperature. The DER 332 resin and PACM curing agent were mixed in the ratio of 28 grams of PACM to 100 grams of DER 332, and degassed at 80°C for 30 minutes under full vacuum.

Substrate: Individual aluminum specimen substrates with dimensions 6cm x 6cm were cut, and an 8 mm pressure-induction hole drilled through the specimen thickness. This hole was subsequently chamfered from the back of the specimen creating a "knife edge" along the top surface of the hole (Figure 8). This sharp edge is critical to initiation of the radial crack once the adherent has been cured.

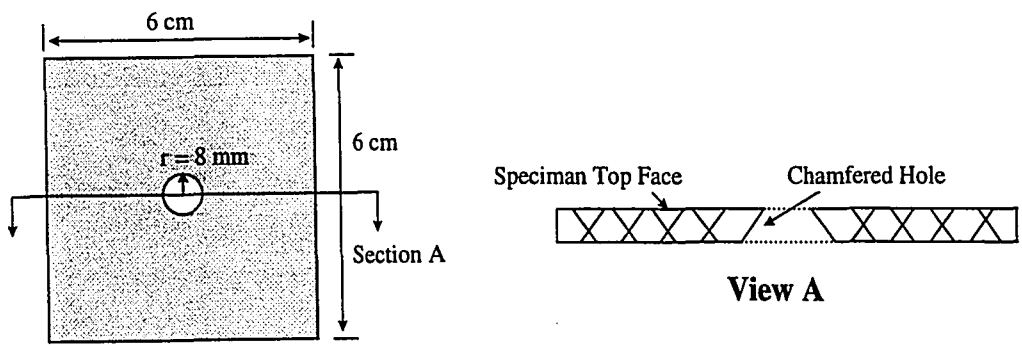

Figure 8 - Schematic Diagram of the Specimen Configuration

Prior to application of the epoxy, the aluminum substrates were ultrasonically cleaned: in (1) a concentrated solution of Alconox (high pH cleaner) for 1 hour, followed by (2) 1 hour in reagent grade acetone. The specimens were removed from the acetone, allowed to air dry and were coated within 2 hours of this cleaning to insure a pristine surface for bonding.

2.3 PRESSURE-INDUCTION HOLE FILLING

Prior to coating of the aluminum substrate with the epoxy coating, the pressure-induction hole was required to be temporarily "plugged" to allow a continuous film to be applied to the specimens surface. The temporary plug was required to be readily removable, and could not damage the epoxy coating during removal. Additionally, the method used to install this plug could not contaminate the surface to be coated, lest erroneous results occur. To this end, a series of techniques and fixtures were developed to allow for precise, repeatable, filling of the pressure-induction hole.

Melted sugar was determined to be the best substance for temporarily filling the hole since it is easily washed away with warm water when required. Creating a "sugar plug" which was smooth and level with the top surface of the specimen required the creation of a fixture to hold the aluminum substrate as heat was applied to the plate and sugar added from the back side of the specimen. Figure 9 depicts this fixture atop a hot-plate which was used to melt the sugar - allowing it to fully fill the hole.

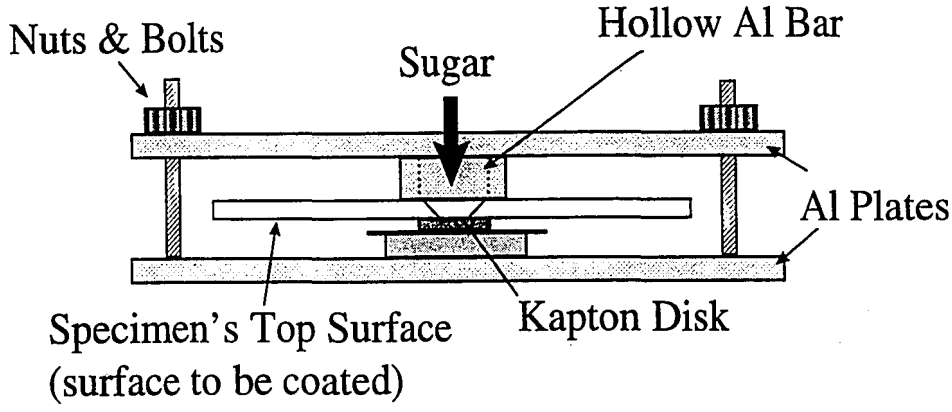

Figure 9 - Sugar Plug Application Fixture

Once the sugar had melted, and the cavity was full (approximately 1 minute), the fixture was removed from the hot-plate, and allowed to air cool. Once cooled, the fixture was removed and a skim coating of DER 332/PACM diluted with acetone (10:1) was applied to the top surface of the sugar plug using a fine modeler's paint brush. This skim coat was the cured for 1 hour at 80° C after which the specimen was ready for coating. This step was necessary because without the intermediate layer on the sugar, the epoxy coating applied to the surface of the specimen was repelled from the sugar plug, yielding an specimen with no epoxy covering the pressure-induction hole.

2.4 COATING APPLICATION

Two techniques were used in the coating of the aluminum substrates. Specimens with coating thicknesses of 254.0, 355.6, 457.2, 558.8, and 660.4 μm were coated using a Gardner knife (Figure 10). This apparatus, a precisely controlled (via

micrometer-like cams) screed allowed for the accurate application of desired coating thicknesses. In order to allow for coating of the entire top surface of the specimen, a special vacuum operated fixture was developed which held the aluminum plate flat and steady while the Gardner Knife was pulled across its surface leaving behind a flat layer of uncured epoxy.

The 76.2 μm specimens were coated using a modeler's airbrush painting system. The specimens were place horizontally flat, and the epoxy was sprayed down at the specimen. Uniform coatings were possible, but the working time of the epoxy once mixed and degassed made this method extremely challenging.

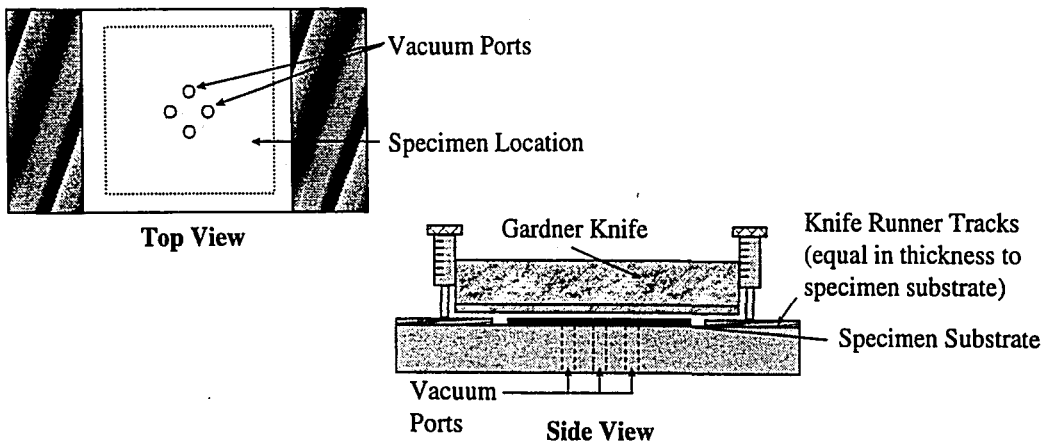

Figure 10 - Gardner Knife / Vacuum Fixture Schematic

2.5 PROCESSING CONDITIONS

After coating, the specimens were placed in an 80° C preheated oven on an aluminum tray which had been leveled previously to maintain uniform coating

thickness over the specimens' surface. The specimens were cured for two hours at this temperature, at which time they were removed from the oven and placed in rapidly stirred 80° C water to remove the sugar plug. (If the sugar plug was not removed prior to the elevated temperature portion of the cure, the sugar would decompose into a non-water-soluble material, which was impossible to remove from the specimen without damaging the epoxy coating.) The specimens were then placed back in the oven, and the controls set for 180°C; this allowed for a ramp up rate of approximately 2°C/min. The specimens were held at 180°C for two hours, at which point the oven was shut off and allowed to slow-cool over night. The specimens were then removed from the oven, and checked for; coating uniformity, surface/interface flaws, and coating thickness. If any problem were found, the specimens were not used in this study.

Coating thickness uniformity and thickness was determined using an *Minitest-2000* ultrasonic coating-thickness gauge manufactured by the P.N. Gardner Company. Eight equally spaced measurements were made of specimen's coating thickness. The average of the measurements was used in all calculations for that specimen. Specimens which exhibited wild fluctuations in coating thickness were not used.

2.6 CRACK INITIATION TECHNIQUE

Even with the knife-edge-like hole edge, an additional "crack initiation" step was required to ensure interface crack propagation without coating failure. Inevitably, a small amount of resin would force its way past the sugar plug and onto the knife edge. This allowed for the polymer to latch onto the perimeter of the hole enough to

stop the initiation of the interfacial crack. A method was developed which utilized a hypodermic needle point to gentle scrape away the offending material, and to initiate a circular crack front parallel to the hole's radius. This technique was applied to each specimen prior to test, but after environmental exposure; thereby eliminating an additional path (through the hole to the interface) for environmental attack to occur.

2.7 ENVIRONMENTAL EXPOSURE

In order to determine the effect that altering the interfacial fracture toughness , K_{ic}, of the interface has on the decohesion parameter, the interface was weakened through environmental exposure. A recirculation still was set up for boiling water exposure of the specimens. Specimens were exposed for 0, 12, 24, 36, 48, and 60 hours in order assure a wide range of fracture toughness values. Initial findings for exposure time vs. debond pressure indicated that this range of exposure times would satisfy the requirement for significantly altering the interfacial fracture toughness of the specimens under test (Figure 11).

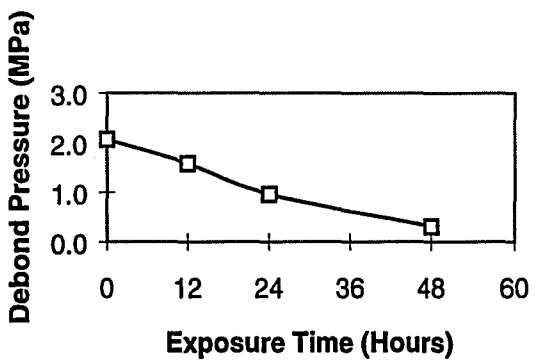

Figure 11 - Exposure Time Determination

2.8 EXPERIMENTAL SETUP

The experimental apparatus used to run the blister tests is comprised of a blister producing fixture and a viewing / measurement system as seen in Figure 12.

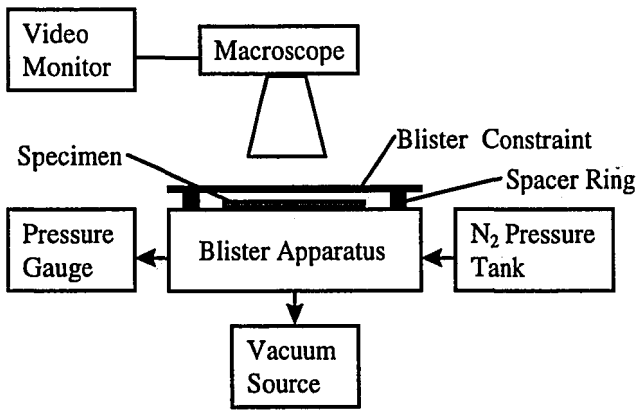

Figure 12 - Schematic Diagram of Experimental Apparatus

The blister fixture (Figure 13) is comprised of a 2 cm thick aluminum plate into which concentric circle rubber seals are let, separating the pressure induction and vacuum port from one another. The vacuum is used to hold the specimen flat during pressurization of the blister with nitrogen gas. National Instrument's LabVIEW for windows was utilized for collection of pressure data. A "Virtual Instrument" (VI) was created which monitored the instantaneous as well as peak pressure being applied to the blister specimen. Pressure data was relayed to the VI via an Omega Engineering Inc. Type PX425 pressure transducer. Pressure was regulated mechanically by means of a high precision manually adjustable regulator. Aluminum spacers rings (0.127 mm and 0.254 mm) were used between the top surface of specimen and the constraining

layer to allow the blister to grow to a predetermined height prior to contacting the constraint. The constraining layer was a aluminum plate with a 6cm x 6cm "window" milled out of its center into which a ¼ inch thick piece of tempered glass was fitted. This setup allowed for the viewing of the specimen as well as for the solid attachment of the constraint which was required while working at the elevated pressures (2+ MPa) utilized during this effort. Additionally, to allow for easier measurement of the radius of the blister coming in contact with the constraint, a thin film of light oil was applied to the bottom surface of the constraining glass. This thin oil film was invaluable for accurate determination of this measurement.

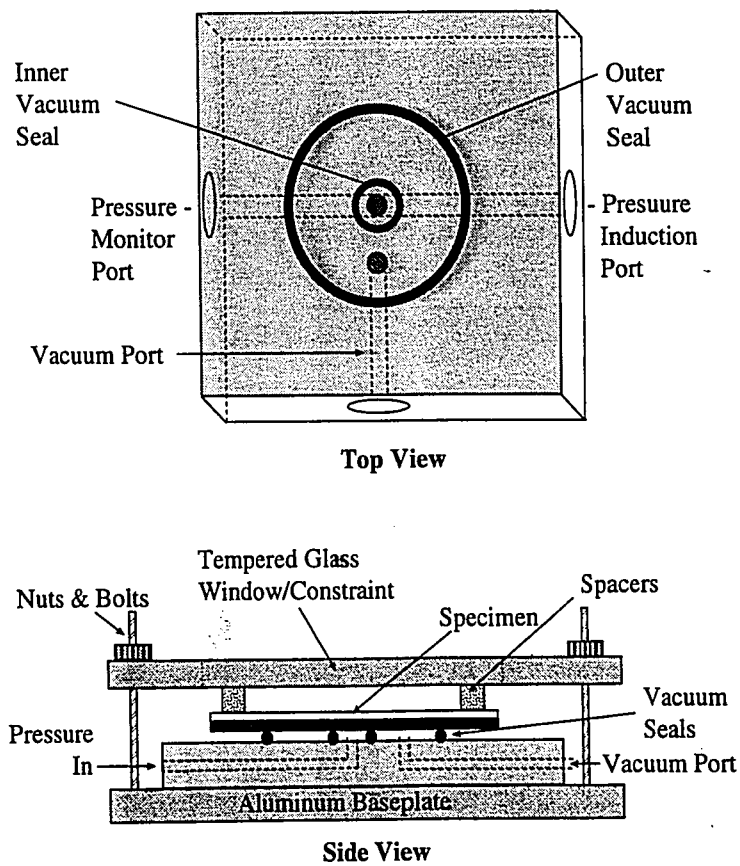

Figure 13 - Schematic Diagram of Blister Fixture

A Nikon SMZ-U metallurgical macroscope was employed for the measurement of the disbond diameter, the constrained diameter, and for the determination of crack growth initiation. Low angle of incidence polarized/green filtered light was utilized to reduce the glare reflecting off the glass constraint layer. The majority of work was performed while viewing the specimen through the macroscope's eyepieces, however, the image was also sent to a video imaging system from which picture of the test could be captured and printed for documentation purposes.

Determination of debond / constrained radii was accomplished through the use of a digital micrometer. Four equally spaced measurements of the diameter for each component were made for each specimen at the point-in-time of crack growth initiation (Figure 14).

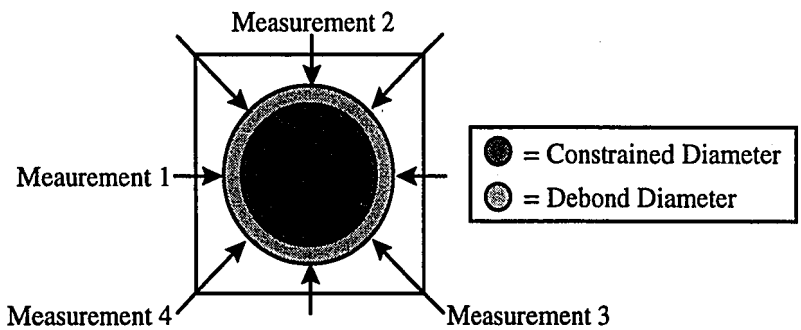

Figure 14 - Schematic of Measurement Locations

The four measurements were averaged, and the average used for calculation of the geometric parameter "q" used in the determination of G_{ic} from Equation 35.

2.9 SPECIMEN TESTING

All testing was conducted at ambient temperature, and testing was performed immediately after environmental conditioning had been completed so as to limit the time during which the specimen could "heal" its weakened interface. A specimen, along with a height spacer, was placed in the constrained blister fixture as described above. The fixture was gently tightened, and vacuum was applied to the underside of the specimen to eliminate shifting during testing. The macroscope was focused on the glass constraint, and N_2 pressure was gradually increased until the interfacial crack began to propagate. At the first sign of crack propagation, the pressure was dumped from the blister via a manual relief valve. The maximum pressure exerted on the blister at the onset of crack propagation was captured, and recorded in a data log by the labVIEW virtual instrument. The disbond region was then measured directly from the specimen (an obvious color change was visible in the disbonded region) while viewing the calipers and specimen through the macroscope. The constrained diameter was measured from the replicate left on the surface of the light oil coated on the inner face of the glass constraining layer. Once these data points were taken the blister was grown slightly to allow for a second measurement-set to be taken from each specimen. The above process was repeated for the second measurement, as well as for two additional specimens per coating-thickness/environmental exposure conditions. A total of 108 specimens - for a total of 216 possible data points - were tested for this

study. A photograph of a common constrained blister specimen during testing is shown in Figure 15 below.

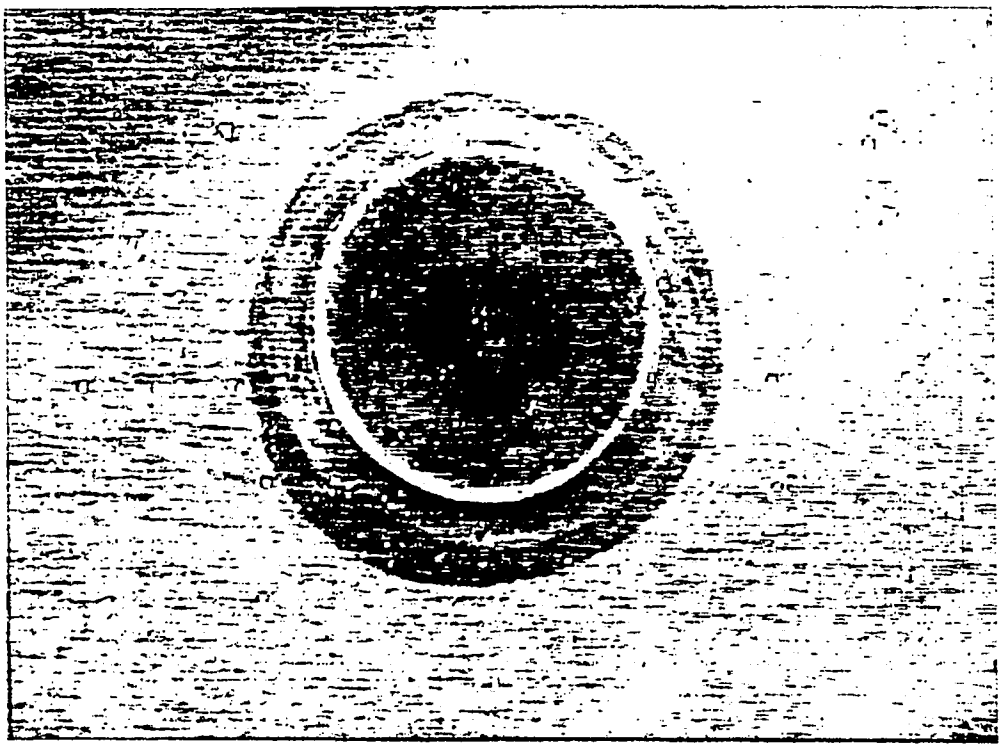

Figure 15 - Photo of Constrained Blister Specimen During Testing

3. RESULTS

Because of the uncertainty of utilizing the Stress Intensity Factor approach to investigate the requirements for fracture at an interface, the Energy Balance Approach was used for this study. However, the decohesion parameter model which we are attempting to utilize to relate coating thickness and residual stress, is based on the Stress Intensity Factor approach. Because of these two requirements, we were forced to work within the Energy Balance Approach in the laboratory, with subsequent conversion of the results into Stress-Intensity-based values. To this end,

experimentally derived values for G_{ic} were determined, converted into K_{ic} values via a bimaterial interface factor based on the modulus of the two materials creating the interface, as outlined in Section 1.4 of this paper, and the common $G_{ic} \rightarrow K_{ic}$ relationship:

$$G_{ic} = \frac{K_{ic}^2}{E} \tag{37}$$

Such an analysis ignores the mixity due to the modulus mismatch at the bimaterial interface and is admittly an approximation. In addition to K_{ic} values, values for residual stress, σ_0, and coating thickness, h, are also required for the examination of the decohesion parameter model under investigation.

3.1 DETERMINATION OF G_{ic}

Experimentally determined values for coating thickness, crack diameter "2a", contact diameter "2d", blister height "h", and debond pressure were utilized in the determination of G_{ic} for each specimen. The "q-factor" outlined in Equation 36 was then individually calculated for each specimen. This q-factor, along with the measured debond pressure and blister constraint height were then inserted in Equation 35, and a G_{ic} for the specimen determined. Individual specimen data are tabulated in Appendix A, with averaged data for each coating thickness / environmental exposure condition

summarized in Appendix B. G_{ic} values were determined to range from a high of 225 J/m^2 for the thickest to 105 J/m^2 for the thinnest - successfully tested (254.0 μm) - unexposed specimens. G_{ic} values for the longest exposure (60 hours) ranged from a high of 115 J/m^2 to a low of 28 J/m^2. Figure 16 shows G_{ic} plotted as a function of boiling-water exposure time for the 6 epoxy coating target thicknesses (actual coating thicknesses for each specimen were used in the calculation of the G_{ic} values for a given "target thickness"). The 76.2 μm specimen all failed prior to propagation except for one specimen which is shown as a square in Figure 16, and appears to hold to the same trend as the other thickness'.

Throughout the range of thicknesses and boiling water exposure, the q factor remained quite constant, with values varying from a low of 0.4107 to a high of 0.4980. This small variation which translates into uniformity from test to test acts as positive self-check of the procedures developed for this work. Had a large disparity existed in q-factors from specimen to specimen, then a non-uniform test protocol would most likely have been the cause of the variance.

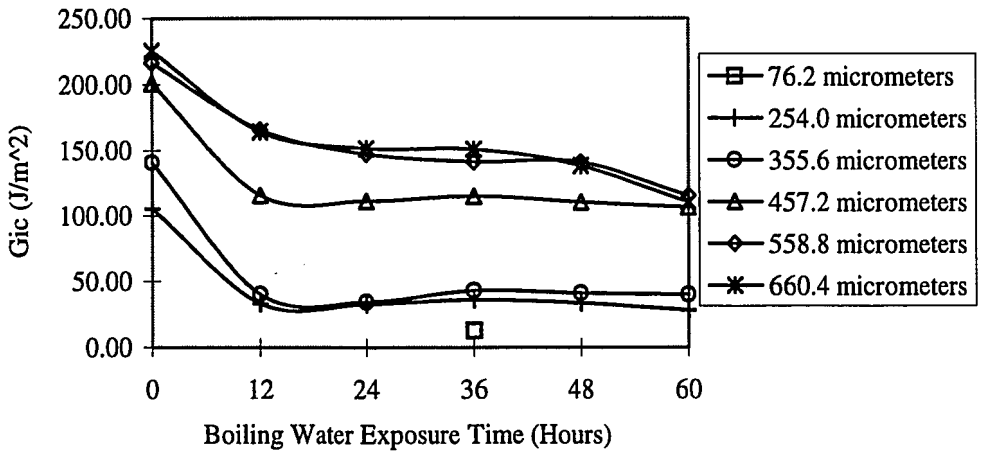

Figure 16 - G_{ic} as a Function of Boiling Water Exposure

Figure 16 shows two distinct trends in the data; a dependence of G_{ic} on boiling-water exposure time, and a dependence of G_{ic} on coating thickness. For each coating thickness, unexposed specimens exhibited significantly greater G_{ic} values than those which had been exposed to boiling water. As the coating thickness increased, the rapidity of the reduction in G_{ic} as a function of exposure time reduced, with the four thinnest samples seeming to reach a lower G_{ic} plateau after 24 hours of exposure, while the two thickest samples required greater than 48 hours to reach this plateau.

Note that the plateaus plotted in Figure 16 show that G_{ic} is a function of the coating thickness. Presumably, the inteface itself is the same for all of the coatings so there must be a geometrical influence. Interestingly, the thin coatings are not as

mechanically contrained as thicker coatings and have a lower residual stress yet these interfaces exhibit the lowest G_{ic} values. There have been arguments in the literature that thin polymer coatings behave as if they are more constrained due to entropic effects from bonding to the rigid surface. However, such effects occur at the nanometer scale and our thinnest coating was 76 microns. Therefore, we shall turn our attention to using the decohesion parameter approach to explain the relationship between fracture toughness, coating thickness, and residual stress.

3.2 CONVERSION OF G_{ic} to K_{ic}

In order to employ the information derived from the blister test, the critical decohesion parameter model requires that the G_{ic} values be converted to K_{ic} values. Equation 17 allows for this conversion to take into account bimaterial interactions in a manner consistent with current bimaterial interfacial fracture theory. Averaged data for each coating thickness and environmental exposure are tabulated in Appendix C, and are plotted in Figure 17. As expected, the K_{ic} data follows the same trends that the G_{ic} data does, with values for the unexposed specimens ranging from 1.06 $MN/m^{3/2}$ for the thickest specimen to 0.75 $MN/m^{3/2}$ for the thinnest (254.0 μm)

specimen. K_{ic} values for the longest exposure (60 hours) ranged from a high of 0.77 $MN/m^{3/2}$ to a low of 0.39 $MN/m^{3/2}$.

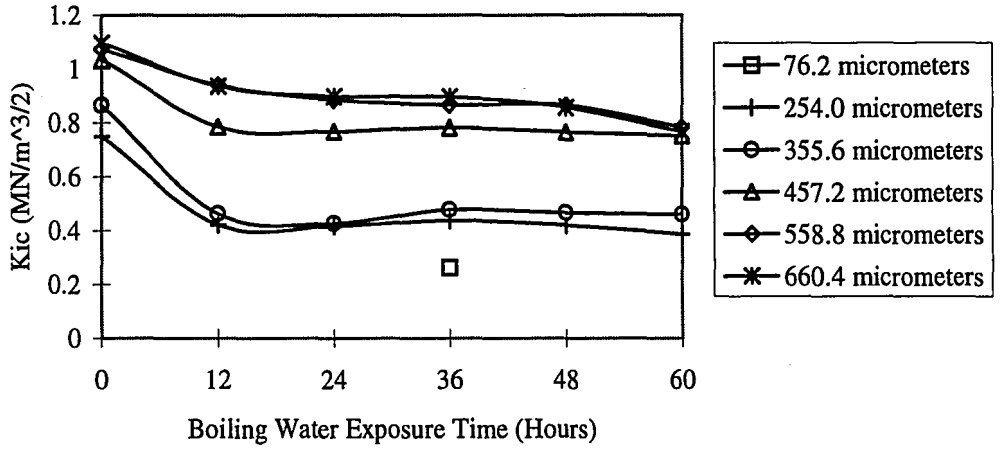

Figure 17 - K_{ic} as a Function of Boiling Water Exposure

To further investigate the interfacial fracture toughness characteristics, K_{ic} was plotted as a function of coating thickness for each of the exposure conditions (Figure 18). Data from each of the exposure conditions followed a similar trend, with K_{ic} increasing in a sigmoidal fashion as the coating thickness increased. Unexposed specimens showed significantly greater K_{ic} values for all coating thicknesses when compared to the other five exposure conditions. Additionally, exposed thick-coated specimens exhibited a reduction in K_{ic} with increased exposure time, while the thinner

coatings (< 457μm) showed little variance with increased exposure. This tendency suggests that substantial interfacial degradation occurred rapidly (≈ 12 hours) in the thinly coated specimens vs the gradual reduction in interfacial integrity apparent in the thicker specimens.

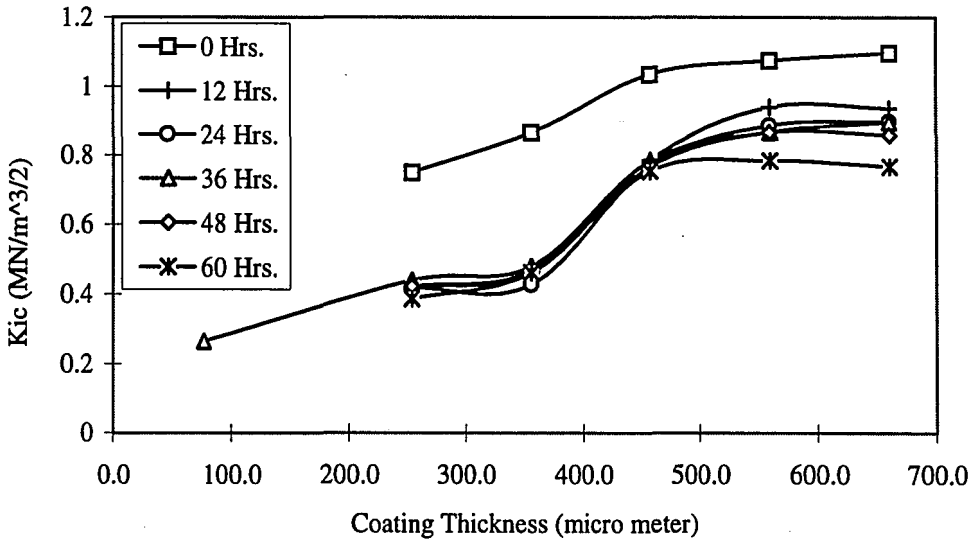

Figure 18 - Kic as a Function of Coating Thickness

3.3 RESIDUAL STRESS CALCULATION

Due to the shrinkage of the organic polymer coating during cure, and the CTE mismatch of the coating and the aluminum substrate during cool down, stresses were within the sample were developed at the time of cure. P. H. Tsao, A. S. Voloshin, and R.A. Pearson[42] have shown that of these two contributors to residual stress, the CTE

mismatch is responsible for the overwhelming majority (>95%) of the demonstrated residual stress. With this in mind, the out-of-plane displacement, or surface curvature "κ", can be determined numerically from beam theory through use of Equation 38 below:

$$\kappa = \frac{(\alpha_1 - \alpha_2)\Delta T}{2\left[\frac{1}{A_1 E_1^0} + \frac{1}{A_2 E_2^0} + \frac{(h_1 + h_2)^2}{4(E_1^0 I_1 + E_1^0 I_2)}\right]} \cdot \frac{h_1 + h_2}{E_1^0 I_1 + E_1^0 I_2} \tag{38}$$

where; E_1^0 and E_2^0 are the biaxial modulus, α_1 and α_2 are the coefficients of thermal expansion, h_1 and h_2 are the thickness', A_1 and A_2 are the cross sectional areas, I_1 and I_2 are the moments of inertia for the aluminum substrate and epoxy coating respectively, and ΔT is the change in temperature the specimen experienced during cure (156° for all specimens in this effort). From this value the residual stress in the epoxy layer can be calculated using beam theory assuming $E_{epoxy} << E_{aluminum}$ through use of Equation 39.

$$\sigma_e = \frac{\kappa E_1^0 t_1}{6\left[1 + \frac{t_2}{t_1}\right]\frac{t_2}{t_1}} \tag{39}$$

where κ, E_1^0, and t_1 are the curvature constant, biaxial modulus of the aluminum substrate and the thickness of the aluminum substrate respectively, and t_2 is the thickness of the epoxy coating.

These equations were used to determine the residual stress present in each of the six thickness of coatings investigated during this effort. The values determined for the specimens ranged from a low of 5 MPa for the thinnest coated specimens, to almost 27 MPa for those at the thicker end of the coating spectrum. A plot of residual stress vs. coating thickness for materials and thickness ranges utilized is shown in Figure 19. These values were used in the determination of the decohesion numbers.

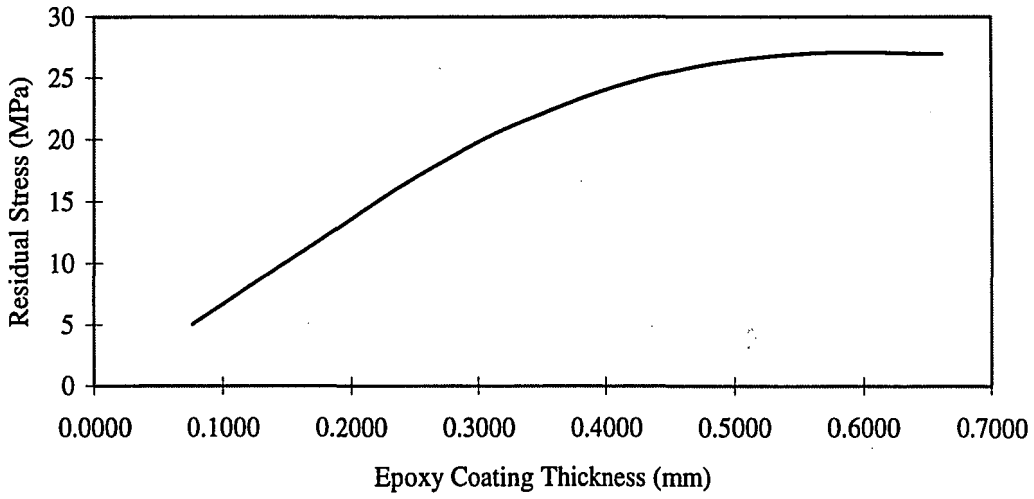

Figure 19 - Residual Stress After Cure vs. Coating Thickness

3.4 CRITICAL DECOHESION NUMBER DETERMINATION

As detailed in section 1.2 the critical decohesion number "Ω_c" can be obtained from the relationship:

$$\Omega_c = K_c / \sigma_o \sqrt{h} \qquad (1)$$

where K_c is the fracture resistance of the interface, σ_o is the residual stress in the coating, and h is the coating thickness. Values for the interfacial fracture toughness determined from the blister test, combined with residual stress values determined numerically and coating thickness' of each specimen allowed for the determination of decohesion numbers for each coating thickness / environmental exposure combination. Appendix D tabulates the summarized finding, with Figures 20 presenting the data in graphical form.

As with the experimentally determined G_{ic} data, the critical decohesion numbers also follow two distinct trends; a dependence of Ω_c on boiling-water exposure time, and a dependence of Ω_c on coating thickness. Firstly, for each coating thickness, unexposed specimens exhibited significantly greater Ω_c values than those which had been exposed to boiling water. Increased exposure times for a given coating thickness also lead to decreased decohesion numbers throughout the thickness range investigated. Secondly, as coating thickness increased, the critical decohesion number decreased, rapidly at first (Demonstrated by the 36 hour exposure time sample group - the only group which included a data point for the thinnest, 76.2 μm, coating.) followed by a more gradual reduction with increased coating thickness.

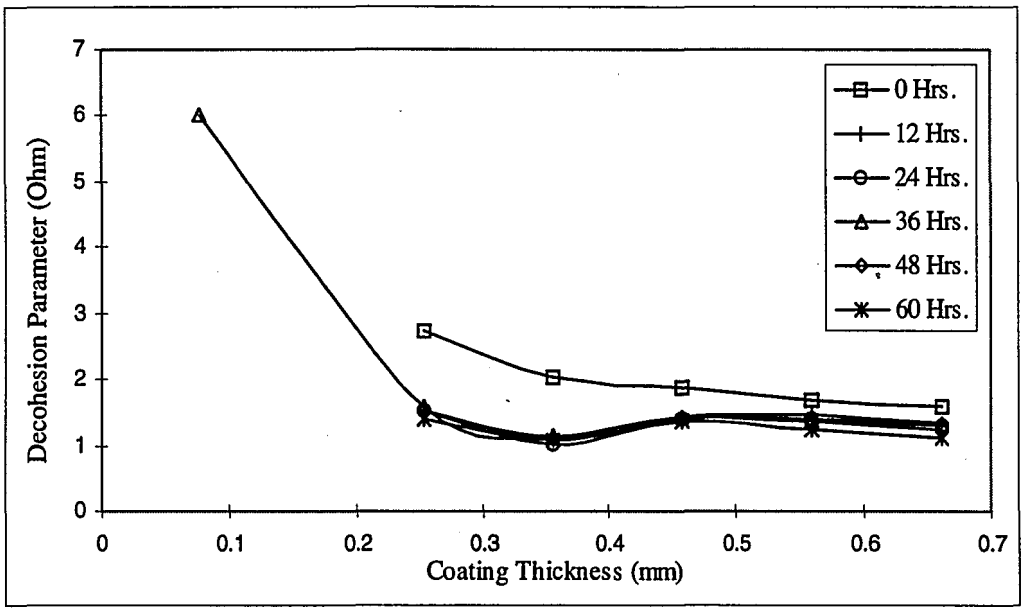

Figure 20 - Ω_c as a Function of Coating Thickness

Critical decohesion number values were found to range from a high of 6.01 (unexposed, 76.2 μm specimen) to a low of 1.01 (24 hour exposure, 355.6 μm specimen), with the majority of points falling in the 1 to 3 range, which is in good agreement with the limited published values for critical decohesion numbers[26].

4. DISCUSSION

4.1 DECOHESION PARAMETER DISCUSION

The overall goal of this study was to investigate the bimaterial interfacial failure of a ductile adherent on a ductile substrate, through use a non-dimensional decohesion parameter model originally developed for use in brittle to brittle bimaterial interfacial fracture work. This model attempts to correlate interfacial fracture

toughness K_{ic}, residual stress σ_O, and coating thickness, h, into the dimensionless critical decohesion number, Ω_C through the equation:

$$\Omega_c = \frac{K_c}{\sigma_0 \sqrt{h}} \tag{1}$$

If the critical decohesion parameter is valid for a given interfacial failure, then the decohesion number obtained from experimental data should be a constant that reflects the influence of both coating thickness and residual stress. If this is not the case, and Ω_c varies as a function of coating thickness, then the critical decohesion parameter - as defined above - can not be applied to the interface under question.

As presented in Figure 20, the critical decohesion parameter for a DEGBA/2024-T3 interfacial failure, was found to vary as a function of coating thickness. This variation of Ω_C with coating thickness questions the applicability of the critical decohesion parameter as a viable tool for the characterization of interfacial failure in the case of a ductile-to-ductile bimaterial interface.

To rule out a plane-strain to plane-stress transition as a cause of decohesion parameter variability, analytical analysis of specimen geometry was performed. All specimen (with the exception of 4 of the unexposed-condition specimens) were estimated to be in a plane-strain condition during the blister-test fracture toughness testing through use of Equation 40.

$$t > 2.5\left(\frac{K_q}{\sigma_y}\right)^2 \tag{40}$$

where, plain strain conditions are met if t, the coating thickness, is greater than 2.5 times the quotient of fracture toughness divided by yield stress squared. As a additional check, coating thickness for all specimens were found to be well in excess of the crack-tip plastic zone size estimates which were calculated using Equation 41:

$$r_y \approx \frac{1}{6\Pi}\frac{K_c^2}{\sigma_{ys}} \text{ (Plane Strain)} \tag{41}$$

where r_y is the damage zone radius, K_c is the fracture toughness, and σ_{ys} is the yield stress of the coating.

4.2 COMPARISON OF G_{ic} VALUES

The interfacial G_{ic} results determined during this research (through use of the constrained blister test) compare favorably to polymer / aluminum interfacial G_{ic} values presented in the literature. Values obtained in this effort range from a low of 13 J/m^2 to a high of 225 J/m^2. Kinloch, Thrusabanjong, and Williams[31] investigated an epoxy / aluminum interfacial toughness, through use of the Symetrical Bimaterial (SBM) specimen. Their values ranged from a low of 32 J/m^2 to a high of 250 J/m^2 with effective toughness ($G_{i\text{-}eff}$) increasing with increased post-cure temperature.

Allen and Senturia[37] investigating polyimide / aluminum interfaces using the island blister test determined the work of adhesion of several polyimide coatings (film thicknesses of ≈ 4.5μm) to range from a low of 90 J/m^2 to a high of 490 J/m^2. While Mostovoy and Ripling[43] determined G_{ic} for an epoxy / aluminum interface submerged in water to be 15 J/m^2.

4.3 COMPARISON OF RESULTS WITH OTHER APPLICATIONS OF Ω_c

Kodnani, Grilo, Pearson, Tsao, and Voloshin[44] investigated the intergrity of polymer / inorganic substrate adhesion using the critical decohesion parameter model. The effect of residual stress and humidity exposure on adhesion of polyimide to silicon was characterized using microindentation fracture toughness testing. The interaction between coating thickness, residual stress induced during processing, and the interfacial fracture toughness was determined using the critical decohesion number, Ω_c. A value of 6.9 was determined for Ω_c , for coating thicknesses in the 20 - 45 μm ranges. This value, as expected due to the superior bonding attributes of the polyimide / silicon interface, is higher than those obtained for the epoxy / aluminum interface. It, is however, in excellent agreement with the thinnest epoxy coating (76 μm) / aluminum value of 6.0.

5. CONCLUSIONS

Based on the results of these experiments and the evaluation of the critical decohesion number model, the following conclusions can be made.

1. A repeatable, precise method for the determination of bimaterial interfacial strain energy release rate, G_{ic}, through the use of the constrained blister test has been developed.
2. The strain energy releases rate, G_{ic}, has been shown to exhibit a dependence on environmental exposure, with G_{ic} decreasing as a function of increasing exposure time.
3. The strain energy releases rate, G_{ic}, has been shown to exhibit a dependence on the thickness of the adhered coating, with G_{ic} increasing as a function of increasing coating thickness.
4. Fracture toughness, K_{ic}, has been shown to exhibit the same dependencies as the strain energy release rate, G_{ic}.
5. The dependence of the critical decohesion number, Ω_c, on environmental exposure times was established, with Ω_c decreasing as exposure time increased.

6. A dependence of the critical decohesion number, Ω_C, on adhered coating thickness was shown, with Ω_C decreasing as coating thickness increased.

7. The critical decohesion number equation: $\Omega_c = \frac{K_c}{\sigma_0\sqrt{h}}$ investigated in this effort was not able to be applied to the ductile-to-ductile (epoxy / aluminum) bimaterial interface fracture toughness case investigated during this effort.

6. FUTURE WORK

Work completed during this research effort has laid a solid experimental foundation for the use of the constrained blister test for investigation into real-world bimaterial interfacial failure. The apparatus as specified in the section 2.8, however, could be improved through the incorporation of a real-time vision system for the measurement of both the crack front and the constrained portion of the blister. Through the incorporation of a vision system, irregularities in blister shape could easily be overcome by determining the crack front length, not by measurement of diameters, but through measurement of actual crack front circumference. The same holds true for the measurement of the constrained portion of the blister. This would allow for a more accurate q-factor to be determined, which would correlate to a more accurate determination of the strain energy release rate for the interface.

As a direct follow-on to this effort, an investigation into varrying the residual stress variable in the critical decohesion number equation should be undertaken. By varying the residual stress within a given coating thickness group, or maintaining the residual stress constant throughout a range of coating thicknesses, the investigation into the applicability of the critical decohesion number model to ductile-ductile interfaces would be complete. As an additional step, the residual stress, instead of being numerically determined for each thickness/cure temperature combination, should be measured to fully justify the accuracy of the model.

Future areas of research should expand the work initiated here to include characterization of like coatings on different substrates, such as copper, titanium, or

organic matrix composites, as well as different classes of coatings such as elastomers, or high temperature polymers. They should also include work focusing on thinner coatings so prevalent in the semiconductor and computer industries. A more suitable technique for application of thin films to the substrate, as well as an improved method for crack initiation for these delicate specimens needs to be developed.

An additional area of research which would exploit the unique nature of the blister test is the crack growth in the presence of an aggressive environment such as water, industrial fluids, or body serums. In these cases the nitrogen gas normally used to apply pressure would be replaced by the fluid in question. The interfacial crack growth could then be monitored as a function of pressure versus time, and a profile of the susceptibility of the bond to environmental attack could be established.

7. REFERENCES

[1] J.W. Smith, E.J. Kramer, F. Xiao, C.Y. Hui, *Measurement of the Fracture Toughness of Polymer-Nonpolymer Interfaces*, Journal of Materials Science, pp. 4234-4244, 1993.

[2] M.E. Thurston, A.T. Zehnder, *Experimental Determination of Silica/Copper Interfacial Toughness*, Acta Metall. Mater., Vol. 41, No. 10, pp. 2985-2992, 1993.

[3] H.C. Choi, K.S. Kim, *Analysis of the Spontaneous Interfacial Decohesion of a Thin Surface Film*, J. Mech. Phys. Solids, Vol. 40, N0.1, pp. 75-103, 1992.

[4] J. Zhang, J.J. Lewandowski, *Interfacial Fracture Toughness Measurement Using Indentation*, Journal of Materials Science, Vol. 29, pp. 4022-4026, 1994.

[5] A.G. Evans, J.W. Hutchinson, *On the Mechanics of Delamination and Spalling in Compressed Films*, Int. J. Solids Structures, Vol. 20, No. 5, pp. 455-466, 1984.

[6] A.G. Evans, J.W. Hutchinson, *Effects of Non-Planarity on the Mixed Mode Fracture Resistance of Bimaterial Interfaces*, Acta Metall., Vol. 3, pp. 909-916, 1989.

[7] J.A. Hinkley, *A Blister Test for Adhesion of Polymer Films to SiO_2*, J. Adhesion, Vol. 16, pp. 115-126, 1983.

[8] A.N. Gent, L.H. Lewandowski, *Blow-off Pressures for Adhering Layers*, Journal of Applied Polymer Science, Vol. 33, pp. 1567-1577, 1987.

[9] H.M. Jensen, *The Blister Test for Interface Toughness Measurement, Engineering Fracture Mechanics*, Vol. 40, No. 3, pp. 475-486, 1991.

[10] K.R. Jiang, L.S. Penn, *Use of the Blister Test to Study the Adhesion of Brittle Materials. Part I. Test Modification and Validation*, J. Adhesion, Vol. 32, pp. 203-216, 1990.

[11] K.R. Jiang, L.S. Penn, *Use of the Blister Test to Study the Adhesion of Brittle Materials. Part Application*, J. Adhesion, Vol. 32, pp. 217-226, 1990.

[12] K.M. Liechti, Y.M. Liang, *The Interfacial Fracture Characteristics of Bimaterial and Sandwich Blister Specimens*, International Journal of Fracture, Vol. 55, pp. 95-114, 1992.

[13] Y.Z. Chu, C.J. Durning, *Application of the Blister Test to the Study of Polymer-Polymer Adhesion*, Journal of Applied Polymer Science, Vol. 45, pp. 1151-1164, 1992.

[14] H.S. Jeong, R.C. White, *Variational Principle of Thin Film Adhesion*, J. Vac. Sci. Technology, Vol. 11, No. 4, 1993.

[15] M.J. Napolitano, A Moet, *Dissipative Processes in Interfacial Failure*, J. Adhesion, Vol. 33, pp. 149-167, 1991.

[16] J.L. Liang, J.P. Bell, A. Mehta, *Adhesion (Fracture Energy) of Electropolymerized Poly(n-octl maleimide-co-styrene) Coatings on copper substrates Using a Constrained Blister Test*, J. Adhesion Sci. Technol., Vol. 7, No.8, pp. 869-884, 1993.

[17] R.W. Hoffman, Phys. Thin Films Vol. 3, p. 211, 1966

[18] M. Janda, Thin Films Vol. 142, p. 37, 1986.

[19] A.G. Evans, J.W. Hutchinson, Int. J. Solids Struct. Vol. 20, p. 451, 1986.

[20] R.M. Cannon, R.M. Fisher, A.G. Evans, Mater. Res. Soc. Proc. Vol. 54, p. 799, 1986.

[21] M.D. Thouless, A.G. Evans, M.F. Ashby, and J.W. Hutchinson, Acta Metall. Vol. 35, p. 1333, 1987.

[22] M. Hu, M.D. Thouless, A.G. Evans, Acta Metall. Vol. 36, p. 1301, 1988.

[23] M.D. Drory, M.D. Thouless, A.G. Evans, Acta Metall. (no date given).

[24] Z. Suo, J.W. Hutchinson, Harvard Applied Sciences Report, MECH 118 (1988).

[25] M.S. Hu, A.G. Evans, Acta Metall. (no date given).

[26] A.G. Evans, M.D. Drory, and M.S. Hu, *The Cracking and Decohesion of Thin Films*, J. Mater. Res., Vol 3, 1988.

[27] A.J. Kinloch, Adhesive and Adhesives, Science and Technology, Chapman and Hall, New York, NY, 10001, 1987.

[28] A.A. Griffith, Phil. Trans Roy. Soc. ,Vol. A221, p. 163, 1920.

[29] E. Orowan, Rep. Prog. Phys. Vol. 12, p. 185, 1948.

[30] G.R. Irwin Appl. Mater. Res. Vol. 3, p. 65, 1973.

[31] A.J. Kinloch, E. Thrusabanjong, J.G. Williams, *Fracture at Bimaterial Interfaces: The Role of Residual Stress*, Journal of Materials Science, Vol. 26, pp. 6260-6270, 1991.

[32] Yeou-Shin Chang, Yeh-Hung Lai, David A. Dillard, *The Constrained Blister - A Nearly Constant Strain Energy Release Rate Test for Adhesives*, J. Adhesion, Vol. 27, pp. 197-211, 1989.

[33] H. Dannenberg, *Measurement of Adhesion by a Blister Method*, J. Appl. Polymer Science, pp. 125-134, 1961.

[34] Mark G. Allen, Stephen D. Senturia, *Measurement of Polyimide Interlayer Adhesion Using Microfabricated Structures,* Massachusetts Institute of Technology, 1988.

[35] M. L. Williams, J. Appl. Polymer Science, Vol. 13, pp. 29-40, 1969.

[36] David A. Dillard, Yong Bao, *The Peninsula Blister Test: A High and Constant Strain Energy Release Rate Fracture Specimen for Adhesives*, J. Adhesion, Vol. 33, pp. 253-271, 1991.

[37] M.G. Allen and S.D. Senturia, J. Adhesion, Vol. 25, pp. 303-315, 1988.

[38] Mark G. Allen, Stephen D. Senturia, *Application of the Island Blister Test for Thin Film Adhesion Measurement*, J. Adhesion, Vol. 29, pp. 219-231, 1989.

[39] Yeh-Hung Lai, David D. Dillard, *Numerical Analysis of the Constrained Blister Test*, J. Adhesion, Vol. 33, pp. 63-74, 1990.

[40] G.P. Anderson, S.J. Bennett and K.L. Devries, *Analysis and Testing of Adhesive Bonds*, Academic Press, New York, 1977.

[41] Y.H. Lai and D.A. Dillard, *An Elementary Plate Theory Prediction of Strain Energy Release Rate of the Constrained Blister Test*, J. Adhesion, (no date).

[42] Pei-Haw Tsao, Arkady S. Voloshin and Raymond A. Pearson, *Residual Stresses in an Organic Die-attached Adhesive,* Draft Report, Lehigh University, Bethlehem PA 18015, 1995.

[43] Mostovoy, S., Ripling, E.J. J. Appl. Polymer Sci., Vol. 13, p. 1083, 1969..

[44] Kodnani, R., Grilo, V., Pearson, R., Tsao, Pei-Haw, Voloshin, A., *Delamination of Polyimide-Silicon Interfaces: The Interplay Between Adhesive Strength, Residual Stress, and Coating Thickness*, Lehigh University, Draft Report, 1998.

Individual Specimen Data - 0 Hours Boiling Water Exposure

Desired Coating Thickness (mm)	Measured Coating Thickness (mm)	Crack Diameter "2a" (mm)	Contact Diameter "2b" (mm)	Suspended Region "d" (mm)	Blister Height "h" (mm)	Debonding Pressure "p" (kPa)	"q" Factor	Glc (J/m^2)
0.254	0.2416	9.8650	8.7450	0.5600	0.127	1924	0.481078	117.62
0.254	0.2416	10.5250	9.4725	0.5263	0.127	1786	0.483333	109.70
0.254	0.2510	10.0775	8.4100	0.8338	0.127	1345	0.472422	80.73
0.254	0.2510	10.9225	9.3850	0.7688	0.127	1724	0.476539	104.40
0.254	0.2565	10.7950	9.4975	0.6488	0.127	1896	0.479968	115.66
0.254	0.2565	11.4725	10.2750	0.5988	0.127	1717	0.482603	105.30
0.3556	0.3470	10.2200	9.7700	0.2250	0.254	1110	0.492661	139.01
0.3556	0.3470	12.2100	10.6250	0.7925	0.254	1193	0.478365	145.04
0.3556	0.3556	11.3650	10.4175	0.4738	0.254	1241	0.486105	153.35
0.3556	0.3556	12.6525	10.9875	0.8325	0.254	1200	0.478068	145.79
0.3556	0.3632	10.5075	9.5150	0.4963	0.254	1055	0.484257	129.85
0.3556	0.3632	11.4675	10.1200	0.6738	0.254	1069	0.480416	130.51
0.4572	0.4445	11.0675	10.3125	0.3775	0.254	1958	0.488630	243.21
0.4572	0.4470	11.4225	9.4150	1.0038	0.254	1131	0.470708	135.29
0.4572	0.4572	12.1975	10.3950	0.9013	0.254	1310	0.475371	158.30
0.4572	0.4572	11.0350	9.4750	0.7800	0.254	1738	0.476439	210.42
0.4572	0.4572	12.3125	10.7800	0.7663	0.254	2110	0.479255	257.02
0.5588	0.5639	11.5700	8.5275	1.5213	0.254	1317	0.456173	152.70
0.5588	0.5664	12.8975	10.6575	1.1200	0.254	2048	0.471054	245.19
0.5588	0.5664	11.4175	8.6350	1.3913	0.254	1786	0.459383	208.52
0.5588	0.5664	12.6525	9.8850	1.3838	0.254	2206	0.463545	259.97
0.6604	0.6477	11.9150	10.7550	0.5800	0.254	1758	0.483774	216.20
0.6604	0.6477	12.6150	11.4675	0.5738	0.254	1765	0.484839	217.53
0.6604	0.6629	11.6575	10.2950	0.6813	0.254	1937	0.480520	236.65
0.6604	0.6629	12.7575	11.1300	0.8138	0.254	2006	0.478738	244.16
0.6604	0.6680	12.5625	11.0000	0.7813	0.254	1744	0.479270	212.51

Individual Specimen Data - 12 Hour Boiling Water Exposure

Desired Coating Thickness (mm)	Measured Coating Thickness (mm)	Crack Diameter "2a" (mm)	Contact Diameter "2b" (mm)	Suspended Region "d" (mm)	Blister Height "h" (mm)	Debonding Pressure "p" (kPa)	"q" Factor	Gic (J/m^2)
0.254	0.2421	10.8075	9.5450	0.6313	0.127	600	0.480530	36.63
0.254	0.2421	11.9875	10.2975	0.8450	0.127	496	0.476503	30.06
0.254	0.2469	10.8625	10.0750	0.3938	0.127	738	0.487917	45.75
0.254	0.2469	12.9350	11.5625	0.6863	0.127	641	0.482315	39.31
0.254	0.2616	10.7775	6.2300	2.2738	0.127	296	0.429676	16.19
0.254	0.2616	12.3700	10.4150	0.9775	0.127	517	0.473659	31.13
0.3556	0.3454	11.6350	9.8850	0.8750	0.127	690	0.474932	41.62
0.3556	0.3454	12.1850	10.5100	0.8375	0.127	572	0.477089	34.70
0.3556	0.3495	12.0425	5.9200	3.0613	0.127	745	0.415265	39.30
0.3556	0.3495	14.0900	11.7575	1.1663	0.127	586	0.472410	35.19
0.3556	0.3556	11.0400	9.3900	0.8250	0.127	827	0.475091	49.96
0.4572	0.4445	11.9850	8.8725	1.5563	0.127	1931	0.456717	112.06
0.4572	0.4445	12.9375	9.7925	1.5725	0.127	1965	0.459485	114.75
0.4572	0.4547	11.2750	10.1975	0.5388	0.127	1910	0.484072	117.50
0.4572	0.4547	12.8100	11.0625	0.8738	0.127	1986	0.477264	120.45
0.4572	0.4597	11.5975	8.9175	1.3400	0.127	1882	0.461486	110.40
0.4572	0.4597	12.2775	9.8725	1.2025	0.127	2006	0.467352	119.18
0.5588	0.5512	12.5200	10.0275	1.2463	0.254	1579	0.466820	187.36
0.5588	0.5512	13.7125	11.0075	1.3525	0.254	1441	0.467122	171.10
0.5588	0.5563	11.1775	10.2875	0.4450	0.254	1717	0.486729	212.41
0.5588	0.5563	12.9625	11.1850	0.8888	0.254	1738	0.477146	210.73
0.5588	0.5588	12.5700	9.7250	1.4225	0.254	945	0.462278	111.00
0.5588	0.5588	13.6000	9.9500	1.8250	0.254	869	0.455270	100.54
0.6604	0.6477	11.4600	10.5975	0.4313	0.254	1593	0.487456	197.35
0.6604	0.6477	12.5575	11.3200	0.6187	0.254	1482	0.483576	182.22
0.6604	0.6706	12.5600	9.3950	1.5825	0.254	1124	0.458002	130.84
0.6604	0.6706	13.8575	10.0075	1.9250	0.254	1020	0.453695	117.68
0.6604	0.6706	12.8425	11.1575	0.8425	0.254	1607	0.478133	195.25
0.6604	0.6706	13.6425	11.3575	1.1425	0.254	1351	0.472085	162.17

Individual Specimen Data - 24 Hour Boiling Water Exposure

Desired Coating Thickness (mm)	Measured Coating Thickness (mm)	Crack Diameter "2a" (mm)	Contact Diameter "2b" (mm)	Suspended Region "d" (mm)	Blister Height "h" (mm)	Debonding Pressure "p" (kPa)	"q" Factor	Gic (J/m^2)
0.254	0.2494	9.8275	9.5525	0.1375	0.127	448	0.495336	28.21
0.254	0.2494	11.6600	10.1950	0.7325	0.127	827	0.479059	50.38
0.254	0.2530	11.0775	9.9925	0.5425	0.127	455	0.483676	27.97
0.254	0.2530	12.9900	11.6100	0.6900	0.127	779	0.482294	47.76
0.254	0.2591	11.2950	8.4075	1.4438	0.127	283	0.457393	16.43
0.254	0.2591	12.8025	9.7400	1.5313	0.127	434	0.460131	25.40
0.3556	0.3536	12.3875	10.0125	1.1875	0.127	469	0.468046	27.89
0.3556	0.3536	14.5800	10.8150	1.8825	0.127	421	0.456962	24.43
0.3556	0.3607	12.7025	8.2650	2.2188	0.127	455	0.441777	25.55
0.3556	0.3607	13.5525	8.8525	2.3500	0.127	586	0.442200	32.94
0.3556	0.3658	11.7425	9.0150	1.3638	0.127	738	0.461287	43.25
0.3556	0.3658	12.7025	9.2425	1.7300	0.127	883	0.454602	50.99
0.4572	0.4597	11.6450	9.0874	1.2788	0.127	1820	0.463395	107.20
0.4572	0.4597	12.9750	10.8000	1.0875	0.127	1800	0.472062	107.97
0.4572	0.4623	11.8425	10.7025	0.5700	0.127	1869	0.483956	114.93
0.4572	0.4623	12.9400	11.8400	0.5500	0.127	1848	0.485832	114.10
0.5588	0.5512	11.5025	9.5300	0.9863	0.254	1172	0.471419	140.46
0.5588	0.5512	12.2450	10.4700	0.8875	0.254	1358	0.475840	164.29
0.5588	0.5588	11.9850	9.2100	1.3875	0.254	1241	0.461410	145.56
0.5588	0.5588	13.0425	9.8750	1.5838	0.254	1276	0.459523	148.99
0.5588	0.5588	12.7825	10.2775	1.2525	0.254	965	0.467338	114.67
0.5588	0.5588	13.4600	10.5475	1.4563	0.254	1427	0.463936	168.31
0.6604	0.6655	12.1225	10.8550	0.6338	0.254	1586	0.482574	194.52
0.6604	0.6655	13.2475	11.5875	0.8300	0.254	1669	0.479116	203.21
0.6604	0.6706	12.8825	6.4875	3.1975	0.254	903	0.417265	95.80
0.6604	0.6706	13.6575	8.2275	2.7150	0.254	972	0.433736	107.18
0.6604	0.6716	12.7400	10.1775	1.2813	0.254	1227	0.466477	145.52
0.6604	0.6716	13.3250	11.0475	1.1388	0.254	1338	0.471513	160.32

Individual Specimen Data - 36 Hour Boiling Water Exposure

Desired Coating Thickness (mm)	Measured Coating Thickness (mm)	Crack Diameter "2a" (mm)	Contact Diameter "2b" (mm)	Suspended Region "d" (mm)	Blister Height "h" (mm)	Debonding Pressure "p" (kPa)	"q" Factor	Glc (J/m^2)
0.0762	0.0869	8.1250	6.5000	0.8125	0.127	221	0.466667	13.09
0.2540	0.2461	10.2750	9.3975	0.4388	0.127	765	0.485766	47.25
0.2540	0.2461	11.5325	10.3975	0.5675	0.127	945	0.483597	58.06
0.2540	0.2642	10.3750	8.6925	0.8413	0.127	331	0.472972	19.89
0.2540	0.2642	12.0825	10.0075	1.0375	0.127	552	0.471377	33.05
0.2540	0.2649	10.8580	8.6800	1.0890	0.127	483	0.466568	28.62
0.2540	0.2649	12.4200	9.9925	1.2138	0.127	503	0.467425	29.90
0.3556	0.3454	11.3450	10.6975	0.3238	0.254	359	0.490488	44.70
0.3556	0.3454	12.1675	11.3250	0.4213	0.254	331	0.488460	41.09
0.3556	0.3531	11.0875	8.5450	1.2713	0.254	365	0.461781	42.89
0.4572	0.4470	11.4450	10.3975	0.5238	0.254	958	0.484746	118.09
0.4572	0.4470	12.1975	11.1650	0.5163	0.254	1069	0.485892	131.99
0.4572	0.4496	12.4825	12.2775	0.1025	0.254	986	0.497263	124.62
0.4572	0.4496	16.0075	15.0000	0.5038	0.254	1034	0.489510	128.69
0.4572	0.4572	12.2000	10.5575	0.8213	0.127	1179	0.477561	71.56
0.5588	0.5613	12.4325	9.7200	1.3563	0.254	1200	0.463637	141.39
0.5588	0.5664	11.4850	11.0300	0.2275	0.254	1241	0.493397	155.65
0.5588	0.5664	14.4075	12.8225	0.7925	0.254	1172	0.481665	143.51
0.5588	0.5664	12.0575	9.9125	1.0725	0.254	1138	0.470350	136.02
0.5588	0.5664	13.0325	10.4000	1.3163	0.254	1089	0.466334	129.13
0.6604	0.6502	11.9000	11.1950	0.3525	0.254	1351	0.490126	168.36
0.6604	0.6502	14.9300	13.0175	0.9563	0.254	965	0.478650	117.44
0.6604	0.6528	12.4000	12.2500	0.0750	0.254	1586	0.497984	200.74
0.6604	0.6528	14.4975	13.3250	0.5863	0.254	1510	0.486521	186.74
0.6604	0.6706	12.9000	11.4300	0.7350	0.254	952	0.481008	116.34
0.6604	0.6706	15.3350	13.9525	0.6913	0.254	931	0.484974	114.75

Individual Specimen Data - 48 Hour Boiling Water Exposure

Desired Coating Thickness (mm)	Measured Coating Thickness (mm)	Crack Diameter "2a" (mm)	Contact Diameter "2b" (mm)	Suspended Region "d" (mm)	Blister Height "h" (mm)	Debonding Pressure "p" (kPa)	"q" Factor	Gic (J/m^2)
0.2540	0.0754	11.5875	10.9950	0.2963	0.127	379	0.491478	23.69
0.2540	0.0757	10.3950	9.2175	0.5888	0.127	669	0.481121	40.90
0.2540	0.0757	13.6200	11.6125	1.0038	0.127	586	0.475434	35.41
0.3556	0.2469	10.6175	9.8475	0.3850	0.254	331	0.487913	41.05
0.3556	0.2642	11.9050	9.0175	1.4438	0.254	352	0.459576	41.08
0.3556	0.2642	12.9450	10.7825	1.0813	0.254	338	0.472158	40.55
0.3556	0.2642	11.2175	9.5300	0.8438	0.254	359	0.474928	43.28
0.3556	0.2642	13.4425	10.3625	1.5400	0.254	331	0.461813	38.85
0.4572	0.3480	12.2000	10.5700	0.8150	0.254	1020	0.477732	123.92
0.4572	0.3480	12.9725	11.0650	0.9538	0.254	972	0.475493	117.50
0.4572	0.3564	11.4725	10.1625	0.6550	0.254	1055	0.480969	128.97
0.4572	0.3564	12.5275	10.9525	0.7875	0.254	752	0.479046	91.51
0.4572	0.3658	11.4925	10.7075	0.3925	0.254	862	0.488616	107.04
0.4572	0.3658	12.7675	11.2525	0.7575	0.254	758	0.480223	92.58
0.5588	0.4547	11.1250	10.4100	0.3575	0.254	1220	0.489288	151.78
0.5588	0.4547	11.9550	11.3125	0.3213	0.254	1303	0.491043	162.65
0.5588	0.4572	12.5850	10.9450	0.8200	0.254	1317	0.478281	160.10
0.5588	0.4572	13.8075	11.7075	1.0500	0.254	1303	0.474651	157.22
0.5588	0.4674	12.4625	10.7625	0.8500	0.254	876	0.477265	106.23
0.5588	0.4674	13.5275	11.8975	0.8150	0.254	869	0.479917	105.98
0.6604	0.5537	12.1275	10.8000	0.6637	0.254	1255	0.481756	153.67
0.6604	0.5537	12.8400	11.7375	0.5513	0.254	1289	0.485689	159.18
0.6604	0.5563	13.2025	10.1600	1.5213	0.254	1207	0.461592	141.57
0.6604	0.5563	13.3600	11.8025	0.7788	0.254	1255	0.480570	153.29
0.6604	0.5690	12.9575	7.3875	2.7850	0.254	1076	0.428356	117.11
0.6604	0.5690	14.1100	10.3200	1.8950	0.254	896	0.455233	103.72

Individual Specimen Data - 60 Hour Boiling Water Exposure

Desired Coating Thickness (mm)	Measured Coating Thickness (mm)	Crack Diameter "2a" (mm)	Contact Diameter "2b" (mm)	Suspended Region "d" (mm)	Blister Height "h" (mm)	Debonding Pressure "p" (kPa)	"q" Factor	Gic (J/m^2)
0.2540	0.2616	10.8775	9.9525	0.4625	0.127	690	0.485827	42.57
0.2540	0.2616	11.9875	10.8875	0.5500	0.127	676	0.484706	41.63
0.2540	0.2642	12.1550	9.8350	1.1600	0.127	214	0.468189	12.72
0.2540	0.2642	13.9100	10.8350	1.5375	0.127	262	0.463156	15.42
0.3556	0.3531	10.7925	9.5025	0.6450	0.254	338	0.480079	41.23
0.3556	0.3531	11.6500	9.9000	0.8750	0.254	324	0.474964	39.12
0.3556	0.3607	11.5875	9.7800	0.9038	0.254	338	0.474002	40.71
0.3556	0.3607	12.1500	10.8525	0.6488	0.254	372	0.482202	45.64
0.3556	0.3640	13.7775	8.2075	2.7850	0.254	338	0.432620	37.15
0.3556	0.3640	13.6600	9.2700	2.1950	0.254	310	0.446437	35.21
0.4572	0.4445	11.9275	9.5100	1.2088	0.254	793	0.466220	93.97
0.4572	0.4445	12.6550	10.4575	1.0988	0.254	745	0.471059	89.16
0.4572	0.4496	11.6828	11.4150	0.1339	0.254	1331	0.496180	167.83
0.4572	0.4496	12.6900	12.2625	0.2138	0.254	1241	0.494385	155.96
0.4572	0.4572	12.5475	6.6900	2.9288	0.254	579	0.422196	62.15
0.4572	0.4572	13.7025	7.9300	2.8863	0.254	641	0.429788	70.05
0.5588	0.5588	11.8250	9.8075	1.0088	0.254	1214	0.471564	145.46
0.5588	0.5588	13.6475	12.0625	0.7925	0.254	1138	0.480644	138.99
0.5588	0.5639	12.6925	8.0925	2.3000	0.254	772	0.439597	86.29
0.5588	0.5639	12.9975	8.7000	2.1488	0.254	793	0.444893	89.67
0.6604	0.6680	12.8925	10.8225	1.0350	0.254	1345	0.473240	161.73
0.6604	0.6680	13.5800	11.3000	1.1400	0.254	993	0.472018	119.13
0.6604	0.6706	13.1500	7.7300	2.7100	0.254	827	0.431305	90.71
0.6604	0.6706	13.6750	10.5350	1.5700	0.254	1034	0.461731	121.38
0.6604	0.6706	13.3925	6.2150	3.5888	0.254	703	0.410678	73.41
0.6604	0.6706	13.6225	7.8800	2.8713	0.254	869	0.429742	94.90

Gic Summary Table

	Zero Hrs. Exposure	12 Hrs. Exposure	24 Hrs. Exposure	36 Hrs. Exposure	48 Hrs. Exposure	60 Hrs. Exposure
Coating Thickness: 76.2 micrometer						
Average **Gic** (J/m^2)				13.09		
Standard Deviation				N/A		
Coefficient of Variation				N/A		
Coating Thickness: 254.0 micrometer						
Average **Gic** (J.m^2)	105.57	33.18	32.69	36.13	33.33	28.08
Standard Deviation	13.29	10.10	13.41	13.95	8.79	16.22
Coefficient of Variation	0.13	0.30	0.41	0.39	0.26	0.58
Coating Thickness: 355.6 micrometer						
Average **Gic** (J/m^2)	140.59	40.15	34.17	42.90	40.96	39.84
Standard Deviation	9.26	6.19	10.73	21.50	1.58	3.62
Coefficient of Variation	0.07	0.15	0.31	0.50	0.04	0.09
Coating Thickness: 457.2 micrometer						
Average **Gic** (J/m^2)	200.85	115.72	111.05	114.99	110.25	106.52
Standard Deviation	52.80	4.00	28.40	28.40	15.90	44.63
Coefficient of Variation	0.26	0.03	0.15	0.15	0.14	0.42
Coating Thickness: 558.8 micrometer						
Average **Gic** (J/m^2)	216.60	165.52	147.05	141.14	140.66	115.10
Standard Deviation	47.77	48.88	19.22	9.83	27.01	31.46
Coefficient of Variation	0.22	0.30	0.13	0.07	0.19	0.27
Coating Thickness: 660.4 micrometer						
Average **Gic** (J/m^2)	225.41	164.25	151.09	150.73	138.09	110.21
Standard Deviation	14.06	33.67	44.05	39.23	22.59	31.07
Coefficient of Variation	0.06	0.20	0.29	0.26	0.16	0.28

Kic Summary Table

	Zero Hrs. Exposure	12 Hrs. Exposure	24 Hrs. Exposure	36 Hrs. Exposure	48 Hrs. Exposure	60 Hrs. Exposure
Coating Thickness: 76.2 micrometers						
Kic (MN/m^3/2)				0.2641		
Coating Thickness: 254.0 micrometers						
Kic (MN/m^3/2)	0.7500	0.4205	0.4174	0.4387	0.4214	0.3868
Coating Thickness: 355.6 micrometers						
Kic (MN/m^3/2)	0.8655	0.4625	0.4267	0.4781	0.4672	0.4607
Coating Thickness: 457.2 micrometers						
Kic (MN/m^3/2)	1.0345	0.7852	0.7692	0.7828	0.7665	0.7534
Coating Thickness: 558.8 micrometers						
Kic (MN/m^3/2)	1.0743	0.9391	0.8852	0.8672	0.8657	0.7831
Coating Thickness: 660.4 micrometers						
Kic (MN/m^3/2)	1.0959	0.9355	0.8972	0.8962	0.8578	0.7663

APPENDIX D Kic / Critical Decohesion Number Summary Table

		"Kic" (MN/m^3/2)	Decohesion Parameter "Ohm"
Coating Thickness: 76.2 micrometers			
Residual Stress: 5.0368 MPa			
H_2O Boil Exposure Time:	0 Hrs.	N/A	N/A
	12 Hrs.	N/A	N/A
	24 Hrs.	N/A	N/A
	36 Hrs.	0.2641	6.01
	48 Hrs.	N/A	N/A
	60 Hrs.	N/A	N/A
Coating Thickness: 254.0 micrometers			
Residual Stress: 17.1516 MPa			
H_2O Boil Exposure Time:	0 Hrs.	0.7500	2.74
	12 Hrs.	0.4205	1.54
	24 Hrs.	0.4174	1.53
	36 Hrs.	0.4387	1.61
	48 Hrs.	0.4214	1.54
	60 Hrs.	0.3868	1.42
Coating Thickness: 355.6 micrometers			
Residual Stress: 22.3663 MPa			
H_2O Boil Exposure Time:	0 Hrs.	0.8655	2.05
	12 Hrs.	0.4625	1.10
	24 Hrs.	0.4267	1.01
	36 Hrs.	0.4781	1.13
	48 Hrs.	0.4672	1.11
	60 Hrs.	0.4607	1.09
Coating Thickness: 457.2 micrometers			
Residual Stress: 25.6212 MPa			
H_2O Boil Exposure Time:	0 Hrs.	1.0345	1.89
	12 Hrs.	0.7852	1.43
	24 Hrs.	0.7692	1.40
	36 Hrs.	0.7828	1.43
	48 Hrs.	0.7665	1.40
	60 Hrs.	0.7534	1.38
Coating Thickness: 558.8 micrometers			
Residual Stress: 26.9990 MPa			
H_2O Boil Exposure Time:	0 Hrs.	1.0743	1.68
	12 Hrs.	0.9391	1.47
	24 Hrs.	0.8852	1.39
	36 Hrs.	0.8672	1.36
	48 Hrs.	0.8657	1.36
	60 Hrs.	0.7831	1.23
Coating Thickness: 660.4 micrometers			
Residual Stress: 26.9769 MPa			
H_2O Boil Exposure Time:	0 Hrs.	1.0959	1.58
	12 Hrs.	0.9355	1.35
	24 Hrs.	0.8972	1.29
	36 Hrs.	0.8962	1.29
	48 Hrs.	0.8578	1.24
	60 Hrs.	0.7663	1.11

VITA

Gary C. Neumeister was born September 22 1965 in Glastonbury Connecticut. He graduated with a Bachelors of Science Degree in Materials Engineering from Drexel University in June 1989. Mr. Neumeister is currently employed as a Materials Engineer in the Advanced Polymer Composite and Materials Branch at the Naval Air Warfare Center in Patuxent River, MD.

END

OF

TITLE